https://doi.org/10.5194/hess-2020-369
Preprint. Discussion started: 24 July 2020

Hydrology and Earth System Sciences
Discussions

Signatures of human intervention – or not? Downstream intensification of hydrological drought along a large Central Asian River: the individual roles of climate variability and land use change

Artemis Roodari[1,2], Markus Hrachowitz[1], Farzad Hassanpour[2] and Mostafa Yaghoobzadeh[3]

[1]Department of Water Management, Faculty of Civil Engineering and Geoscience, Delft University of Technology, Stevinweg 1, 2628CN Delft, Netherlands
[2]Department of Water Engineering, Faculty of Soil and Water Sciences, University of Zabol, Zabol, 98615-538, Iran
[3]Department of Water Engineering, University of Birjand, Birjand, 97175-615, Iran

Correspondence to: Artemis Roodari (artemis_roodari@yahoo.com)

Abstract. The transboundary Helmand River basin is the main drainage system for large parts of Afghanistan and the Sistan region of Iran. Due to the reliance of this arid region on water from the Helmand River, a better understanding of hydrological drought pattern and the underlying drivers in the region are critically required for an effective management of the available water. The objective of this paper is therefore to analyse and quantify spatio-temporal pattern of drought and the underlying processes in the study region. More specifically we test for the Helmand River Basin the following hypotheses for the 1970-2006 period: (1) drought characteristics, including frequency and severity systematically changed over the study period, (2) the spatial pattern and processes of drought propagation through the Helmand River Basin also changed and (3) the relative roles of climate variability and human influence on changes in hydrological droughts can be quantified.

It was found that drought characteristics varied throughout the study period, but did largely show no systematic trends. The same was observed for the time series of drought indices SPI and SPEI, which exhibited considerable spatial coherence and synchronicity throughout the basin indicating that, overall, droughts similarly affect the entire HRB with little regional or local differences. In contrast, analysis of SDI exhibited significant negative trends in the lower parts of the basin, indicating an intensification of hydrological droughts. It could be shown that with a mean annual precipitation of ~250 mm y^{-1}, streamflow deficits and thus hydrological drought throughout the HRB are largely controlled by precipitation deficits, whose annual anomalies on average account for ±50 mm y^{-1} or ~20% of the water balance of the HRB, while anomalies of total evaporative fluxes on average only account for ±20mm y^{-1}. The two reservoirs in the HRB only played a minor role for the downstream propagation of streamflow deficits, as indicated by the mean difference between inflow and outflow during drought periods which did not exceed ~0.5% of the water balance of the HRB. Irrigation water abstraction had a similarly limited effect on the magnitude of streamflow deficits, accounting for ~10% of the water balance of the HRB. However, the downstream parts of the HRB moderated the further propagation of streamflow deficits and associated droughts in the early decades of the study period. This drought moderation function of the lower basin was gradually and systematically inverted by the end of the study period, when the lower basin eventually amplified the downstream propagation of flow deficits and

https://doi.org/10.5194/hess-2020-369
Preprint. Discussion started: 24 July 2020


Hydrology and Earth System Sciences
Discussions

droughts. This shift from drought moderation to drought amplification in the lower basin is likely a consequence of increased agricultural activity and the associated increases in irrigation water demand from ~13 mm y^{-1} at the beginning of the study period to ~23 mm y^{-1} at the end and thus in spite of being only a minor fraction of the water balance. Overall the results of this study illustrate that flow deficits and the associated droughts in the HRB clearly reflect the dynamic interplay between temporally varying regional differences in hydro-meteorological variables together with subtle and temporally varying effects linked to direct human intervention.

1 Introduction

The transboundary Helmand River system between Afghanistan and Iran is the primary contributor of water to the Hamun lake- and wetland-system in the Sistan Plain, which is the terminus of one of the largest endorheic basins in Central Asia. In this region, which is described as one of the driest, most remote deserts on Earth (Whitney, 2006), water from the Helmand River system plays a critical role not only to sustain agricultural production, hydropower generation and ecosystem stability but also for drinking water supply for some one million people living in the region, including the cities of Kandahar in Afghanistan and Zabol in Iran.

The area has recently experienced a severe, multi-year drought (1998–2004). Reduction of flow and episodic no-flow conditions in the Helmand River during this period have caused significant disruption of water supply. As a consequence, agricultural production dropped by almost 90% as compared to average no-drought conditions, further resulting in food shortage and considerable economic damage (Ebrahimzadeh and Esmaelnejad, 2013). Given the region's extreme dependence on water from the Helmand River system and the associated vulnerability to hydrological droughts, a few recent studies started to analyse droughts in Afghanistan and the Helmand River Basin (e.g. Ahmad and Wasiq, 2004; Miyan, 2015). For example, Alami et al. (2018) analyzed meteorological droughts in the Helmand River Basin using different methods and quantitatively documented the extreme drought in 2001. However, most of the research in this region focused on the application of hydrological models for the simulation of runoff to provide decision bases for integrated water management issues in the region. These studies include Hajihosseini et al. (2016), who assessed the Afghan-Iranian Helmand River Treaty (The Iranian-Afghan Helmand (Hirmand) River Water Treaty, 1973) using the SWAT model (Arnold et al., 1998) and data from the Climatic Research Unit (CRU; Harris et al., 2014). A study by Wardlaw et al. (2013) formulated a model for the development of water resources systems in the Helmand River Basin using the Water Evaluation and Planning (WEAP) model and established a list of scenarios for the future.

Similarly, Vining and Vecchia (2007) estimated future runoff conditions of the river to evaluate the effects of different reservoir operation strategies under different climate change scenarios on downstream water supply. Van Beek et al. (2008) developed methods and tools to build the capacity to sustain agriculture and ecosystems in the downstream Sistan Plain. In spite of this growing body of literature for the region, the scarcity of reliable meteorological and hydrological data so far

https://doi.org/10.5194/hess-2020-369
Preprint. Discussion started: 24 July 2020


Hydrology and Earth System Sciences
Discussions

limited systematic, quantitative analysis of spatio-temporal pattern of hydrological droughts and the underlying drivers and processes in the Helmand River Basin.

In a world under change, however, decision makers need such quantitative information about drought characteristics to ensure the development and implementation of effective and sustainable water management procedures. To be reliable this information needs to be based on a solid understanding of how different types of droughts propagate through different hydrological systems. While meteorological droughts are controlled by precipitation deficits only, agricultural and hydrological droughts are caused by soil moisture and runoff deficits, respectively. As pointed out, amongst others, by Mishra and Singh (2010) the processes underlying the latter two are complex because they are dependent on many interacting processes in terrestrial hydrological systems, such as the water and release dynamics of the subsurface as well as land-atmosphere exchange. Therefore, monitoring and analysis of hydrological droughts have received increased attention in recent decades (van Huijgevoort et al., 2014; Pathak and Dodamani, 2016; Weng et al., 2015; Vicente-Serrano et al., 2012; Kubiak-Wójcicka and Bak, 2018; Trambauer et al., 2014; Ahmadalipour et al., 2017; Jiao and Yuan, 2019; Moravec et al., 2019). In general, it is well-understood that both, agricultural and hydrological droughts are modulated by the interactions of climate, river basin characteristics, such as geology, as well as human influence or any combination thereof (e.g. Van Lanen et al., 2013; Huang et al., 2016; Liu, et al., 2016; Van Loon, et al., 2019). For example, data show that reservoir operations can have both, considerable positive or negative effects on downstream hydrological drought pattern (e.g. Zhang et al., 2013; Pingue et al., 2016; Wu et al., 2017), which may politically be particularly sensitive for transboundary rivers (Al-Faraj and Scholz, 2015).

Due to the reliance of the region on water from the Helmand River, a better understanding of hydrological drought pattern and the underlying processes in the region are critically required for an effective management of the available water. The objective of this paper is therefore to analyse and quantify spatio-temporal pattern of drought and the underlying processes in the study region. More specifically we will test for the Helmand River Basin the following hypotheses for the 1970-2006 period: (1) drought characteristics, including frequency and severity systematically changed over the study period, (2) the spatial pattern and processes of drought propagation through the Helmand River Basin also changed and (3) the relative roles of climate variability and human influence on changes in hydrological droughts can be quantified.

2 Study area

The endorheic Helmand River Basin (HRB; Figure 1) covers approximately 105,000 km^2 or 15 % of Afghanistan. From its source area, in the Koh-i-Baba mountains, an extension of the Hindu Kush west of Kabul, with elevations to over 4600 masl, the Helmand River system drains into the Hamun lake and wetland system in the Sistan plain of Eastern Iran, a closed inland delta with a minimum elevation of 440 masl in the south-west of the HRB, which covers 5 % of the total HRB area (Goes et al., 2016). Both, long-term mean annual precipitation ($\bar{P}$=90-480 mm yr^{-1}; Figure 1d) and potential evaporation ($\overline{E_P}$ =700-1800 mm yr^{1}; Figure 1e) exhibit considerable spatial variability throughout the HRB. This results in a pronounced gradient

https://doi.org/10.5194/hess-2020-369
Preprint. Discussion started: 24 July 2020


Hydrology and Earth System Sciences
Discussions

of aridity from sub-arid in the North-East to hyper-arid conditions in the South-West as expressed by the aridity index I_A ($I_A = \frac{\bar{P}}{\bar{E}\bar{P}}$ [-]; Figure 1f). Precipitation falls mostly in the winter months and in the upper basin almost always occurs as snow. In general, snowmelt generates the annual runoff peaks in early spring and sustains flow in the HRB throughout the dry summers. For the following analysis, the HRB is divided into six sub-basins (Figure 1c; Table 1): the Upper Helmand River Basin (UHRB) with the main stem of the Helmand River, the Central Helmand River Basin (CHRB) and the Upper Arghandab River Basin (UARB) as well as the Lower Arghandab River Basin (LARB) are nested in and drain into the Lower Helmand River basin (LHRB) and subsequently into the Sistan plain (SISP). The UHRB accounts for 80% of the combined inflow into the LHRB. Flow in the LHRB is influenced by the operation of two upstream reservoirs (Figure 1b; Table 1). While the reservoir at Kajakai Dam with a storage capacity of 1800 mio. m^3, located at the outflow of the UHRB, is a multi-purpose structure for electricity production, flood control and irrigation water supply, the smaller Dahla Dam, located at the outlet of the UARB into the LARB about 180 km upstream of the confluence with the LHRB, has a storage capacity of 450 mio. m^3 and is used mainly for irrigation of the lower Arghandab valley (Goes et al., 2016).

Due to the arid climate, natural vegetation is very scarce and mostly limited to seasonal grassland throughout the entire HRB. Irrigated agriculture is by far the largest consumer of water, accounting for 98 % of all abstractions (Goes et al., 2016). Except for a few recent irrigation projects in the LARB and LHRB, irrigation relies on traditional methods with irrigation canals and is thus largely confined to the valley floors along the main river channels (Figure 1b). While the irrigated area in the LARB remained somewhat stable at around 370 km^2 (~ 0.3 % of the total HRB) over the last decades, satellite imagery (Landsat 7, ETM+) shows that the total irrigated area in the LHRB more than doubled from < 800 km^2 (0.8 %) in the late 1970s to 1650 km^2 (1.6 %) in 2011 (Figure 2). More than 200 km^2 of the increase in irrigated area are due to the conversion of seasonal grasslands to high-water-requirement poppy cultivation since the 1990s (Hajihosseini et al., 2019). By 2006 around 690 km^2 in the HRB were used for poppy cultivation (UNODC, 2006). In 2011, the main crops in the HRB are wheat (~47 %), poppy (~ 32 – 37 %), maize and beans (~16 %), with orchards in some areas (~1–4 %), most of the crops located in the traditionally irrigated areas (Wardlaw et al., 2013).

3 Climatological and hydrological data

The HRB is characterized by a poor coverage of reliable historic in-situ observations of hydro-climatic variables, particularly in the upper parts of the basin where most of the water in the HRB originates from. Analysis of Hajihosseini et al. (2016) indicated that the spatio-temporal variation of the interpolated historical precipitation and temperature in the gridded Climatic Research Unit (CRU) dataset was largely consistent with available ground observations for Afghanistan. Therefore, we here used daily precipitation and temperature estimates for the 1970–2006 study period (Figure 1a), downscaled from the monthly CRU TS 3.10 dataset (Harris et al. 2014), based on the dGen algorithm (Geng et al., 1986) that was previously also applied in other studies (e.g. Schuol and Abbaspour, 2006; Schuol et al., 2008; Hajihosseini et al., 2016). The data were available from www.2w2e.com (Ashraf Vaghefi et al., 2017) at a spatial resolution of 0.5°×0.5°.

https://doi.org/10.5194/hess-2020-369
Preprint. Discussion started: 24 July 2020


Hydrology and Earth System Sciences
Discussions

Daily streamflow observations for the 1970-1979 period are available from the US Geological Survey (waterdata.usgs.gov) at six gauging stations throughout the HRB (IDs 1-2, 4-7; Figure 1; Table 1). Note, that there were observations available from individual gauging stations at the inlets upstream of the Kajakai Dam (ID1 – $UHRB_U$) and Dahla Dam Reservoirs (ID4 - $UARB_U$) as well as at the corresponding outlets downstream of the dams (ID2 – $UHRB_D$; ID5 – $UARB_D$). In addition, monthly flow observations for the 1970-2006 period were available at the inflow to the Sistan Plain (ID8 – SISP).

4 Methods

The analysis of the characteristics and pattern of hydrological droughts in the HRB over the recent decades in this study required a two-step approach. In a first step, the observed streamflow time series (1970-1979; Table 1) had to be extended to cover the full 1970-2006 study period, using a hydrological model. In a second step, the modelled streamflow estimates for the 1970-2006 period at eight locations in the HRB were used to analyse hydrological droughts.

4.1 Hydrological model

We used a distributed implementation of a process-based hydrological model, based on the general concept of the FLEX model-family (e.g. Fenicia et al., 2008; Gharari et al., 2014; Bouaziz et al., 2018) to generate estimates of daily discharge from the sub-basins $UHRB_U$ (ID1), CHRB (ID3), $UARB_U$ (ID4), LARB (ID6), LHRB (ID7) and SISP (ID8). In addition, a simple reservoir routing scheme was used to estimate outflow from the two reservoirs (ID9-10), located at $UHRB_D$ (ID2) and $UARB_D$ (ID5).

4.1.1 Model structure at grid cell scale

The core of the model are five storage components (Figure 3) that are linked by fluxes and that conceptually represent snow storage S_{sn} [mm], interception storage S_i [mm], storage in the unsaturated root-zone S_u [mm], a fast responding component S_f [mm] that generates preferential and overland flow, and a slow responding groundwater storage S_s [mm]. A lag function represents the lag time between storm and flood peak. The snow module is based on a simple degree-day method that has been effectively applied in many conceptual models (e.g. Parajka and Blöschl, 2008; Konz and Seibert, 2010; Gao et al., 2017; Nijzink et al., 2018; Mostbauer et al., 2018). When the average daily temperature is below a threshold temperature T_t [°C], precipitation enters the system as snowfall P_s [mm d^{-1}] and is stored in S_{sn} When there is snow cover and the temperature exceeds T_t, snow melt M [mm d^{-1}], specified by a melt factor F_m [mm $°C^{-1}$ d^{-1}], sets in from S_{sn}. Precipitation falling as rain P_r [mm d^{-1}] first enters the interception reservoir S_i, specified by an interception capacity I_{max} [mm]. Water evaporates as interception evaporation E_i [mm d^{-1}] from S_i at potential rates E_p [mm d^{-1}], while water in S_i that exceeds the storage capacity I_{max} reaches the soil as throughfall P_{tf} [mm d^{-1}]. The total effective precipitation P_e [mm d^{-1}] infiltrating into the unsaturated soil root-zone S_u at any given time step is then the sum of P_{tf} and M (Gao et al., 2014). Water in the unsaturated reservoir S_u is, depending on the storage capacity S_{umax} [mm], either stored and eventually released by plant

https://doi.org/10.5194/hess-2020-369
Preprint. Discussion started: 24 July 2020


Hydrology and Earth System Sciences
Discussions

transpiration E_T [mm d^{-1}], or directly released as groundwater recharge R_s [mm d^{-1}] or preferential flow R_f [mm d^{-1}]. The response reservoirs S_f and S_s represent a fast responding storage component and a slower responding groundwater component, respectively, that both drain water to the river according to their associated time scales k_f [d] and k_s [d], so that that the total flow can be expressed as $Q=Q_f+Q_s$ [mm d^{-1}]. All relevant model equations are provided in Table S1 in the supplementary material.

4.1.2 Reservoir routing

Large reservoirs such as the Kajakai (ID9) and Dahla (ID10) Dam reservoirs in the HRB, can considerably alter downstream flow regimes (Haddeland et al., 2014; Wada et al., 2017). This has recently received growing attention and a number of studies have suggested methods to quantify reservoir outflow where reservoir operation rules are largely unknown (e.g. Coerver et al., 2018; Yassin et al., 2019). Here, the effects of the reservoirs were estimated with a simple water accounting scheme based on elevation-storage and elevation-area relationships provided in a study by Vining and Vecchia, (2007) and similar to previous work (e.g. Hanasaki et al., 2006; Wisser et al., 2010):

$$\frac{dS_r(t)}{dt} = Q_{in}(t) - Q_{out}(t) + P(t) - E_p(t), \quad (1)$$

Where S_r is the reservoir storage, P and E_p are precipitation and potential evaporation over the surface area of the reservoir at the end of the previous time step, respectively. Q_{in} is the inflow to the reservoir, Q_{out} the outflow from the reservoir. Here, the inflows Q_{in} to the two reservoirs were estimated by the hydrological models of the respective upstream sub-basins $UHRB_U$ (ID1) and $UARB_U$ (ID4). Due to the lack of more detailed data, Q_{out} was in this study estimated based on empirical storage-outflow relationships that relate modeled reservoir storage S_r (Eq.1) and Q_{in} to observations of Q_{out}, i.e. Q_{ID2} and Q_{ID5}. We decided to develop separate linear relationships for high- and low-flow seasons, i.e. January to June and July to December, respectively as preliminary analysis suggested that these were more robust than non- or piecewise-linear relationships for the entire year, as used elsewhere (e.g. Yassin et al., 2019):

$$Q_{out} = \begin{cases} a_h S_{r,t-1} + b_h Q_{in,t} + c_h & \rightarrow high\ flow\ season \\ a_l S_{r,t-1} + c_l & \rightarrow low\ flow\ season \end{cases}, \quad (2)$$

Where a [d^{-1}], b [-], c [mm d^{-1}] are coefficients and the subscripts h and l indicate high and low flow seasons, respectively. Note, that Q_{in} becomes negligible in the low flow season and the relationship collapses to a simple linear regression.

4.1.3 Model implementation at (sub-)basin scale

The model was implemented in a distributed way and the flows aggregated to the (sub-)basin scale. To limit the computational requirements, the meteorological input data, available at a spatial resolution of 0.5° x 0.5°, were averaged to run the model at a grid cell size of 1° x 1° (Figure 1). The snow (S_{sn}), interception (S_i) and unsaturated (S_u) reservoirs in each

https://doi.org/10.5194/hess-2020-369
Preprint. Discussion started: 24 July 2020


Hydrology and Earth System Sciences
Discussions

model grid cell were further stratified into 500m elevation bands to account for elevation-dependent snow dynamics and the associated differences in liquid water input to the system. The combined groundwater recharge R_s and the combined preferential drainage R_f from all elevation zones in each model grid cell was then computed as the weighted average from all individual elevation zones, based on the areal proportion of each elevation zone (cf. Fenicia et al., 2008; Euser et al., 2015).

The flow Q_i generated in each of the N grid cells of a (sub-)basin j at any time step t was subsequently routed to the (sub-) basin outlet in a convolution operation with triangular lag functions (e.g. Fenicia et al., 2011) based on lag times τ_i, proportional to the mean flow distances from the individual i cells to the outlet. In addition, irrigation demand I_D [mm d^{-1}] for agriculture was accounted for by direct river water abstractions. The aggregated flow at the outlet of a (sub-)basin was then the sum of all flows routed to the outlet minus irrigation demand, i.e. $Q_{ID_j} = \sum_{i=1}^{N} \left(Q_{i,j} * h(\tau_{i,j})\right) - I_{D,j}$ of that specific (sub-)basin j, i.e. ID1-7. At each time step, irrigation water $I_{D,j}$ was then re-applied as input to $S_{u,i}$ in grid cells i of the corresponding subbasin j that featured agricultural use. Largely being an unregulated irrigation canal system and due to the lack of more detailed information, estimates of $I_{D,j}$ were here based on crop coefficients K_c, potential evaporation E_p and effective precipitation P_e for each day k, as well as the agriculturally used area in each year l (Allen et al., 1998), according to $I_D = K_c\left(E_p - P_e\right)_{k,l} A_l$

As a baseline, crop coefficients and the agriculturally used area were estimated based on crop pattern reported by Wardlaw et al., (2013). In that report, the irrigated areas were estimated using satellite imagery from 2010/2011. To account for land-use change over the 1970-2006 study period, the estimates were adjusted to changes in agricultural area as extracted from available satellite imagery in 1977, 1988, and 1998.

The outflow of sub-basins $UHRB_U$, i.e.Q_{ID1}, and $UARB_U$, i.e. Q_{ID4}, were used as inflow to the Kajakai Dam (ID9) and Dahla Dam (ID10) reservoirs, respectively. The resulting estimates of reservoir outflows, i.e. Q_{ID2} and Q_{ID5} (section 4.1.2) were then used as inflows into LHRB (ID7) and LARB (ID6), respectively. In addition, LHRB (ID7) received the outflows Q_{ID3} and Q_{ID6}, while LHRB (ID7) outflow Q_{ID7} subsequently drained into SISP (ID8).

The historical absence of significant snow cover in the sub-basins ID2 and ID5-8 allowed us to omit the snow component and the related parameters from the model in these sub-basins (Figure 3) and to limit the adverse effects of equifinality (Beven, 2001). Furthermore, as agriculture is largely confined to the sub-basins LARB (ID6) and LHRB (ID7), the redistribution of river water for irrigation was only implemented in these two sub-basins. Similarly, an additional parameter to account for deep infiltration losses k_L was used for the sub-basins ID6-ID8. The above differences resulted in two slightly different implementations of the model in the uplands and the downstream regions of the HRB, respectively, and hereafter referred to as Model-1 and Model-2 (Figure 3). Similar implementations of this model type have in the past proven successful in a range of different environments (e.g. Prenner et al., 2018; Hulsman et al., 2020).

https://doi.org/10.5194/hess-2020-369
Preprint. Discussion started: 24 July 2020


Hydrology and Earth System Sciences
Discussions

4.1.4 Model calibration and post-calibration evaluation

The models were run on a daily time step in all sub-basins for the entire 1970-2006 period. However, in the absence of suitable data, the models could not be calibrated for all sub-basins and over the entire period. Rather, only the models of the five sub-basin outlets $UHRB_U$ (ID1), $UARB_U$ (ID4), LARB (ID6), LHRB (ID7) and SISP (ID8) (Table 1; Figure 3) were
220 individually calibrated for the 1970-1975 period to time series of observed flow. Note, that all model grid cells in a given sub-basin were run with the same parameter sets but with spatially distributed hydro-climatic forcing (e.g. Ajami et al., 2004; Euser et al., 2015). To limit the effects of equfinality (Beven, 2001) and to ensure robust model implementation (Euser et al., 2013; Hrachowitz and Clark, 2017), we adopted a multi-objective (Gupta et al., 1998) calibration approach, simultaneously using the Nash-Sutcliffe Efficiency (Nash and Sucliffe, 1970) of flows ($E_{NS,Q}$) and of the logarithm of flows ($E_{NS,log(Q)}$) as
225 objective functions. The 10 ($UHRB_U$, $UARB_U$) and 8 (LARB, LHRB, SISP) free calibration parameters, respectively, in the individual models were sampled in 10^6 realizations from uniform prior distributions following a Monte Carlo strategy. The model parameters together with their prior and posterior distributions are given Table 2. To account for trade-offs in the multi-objective calibration and uncertainties in the modelling process, we kept all parameter sets that fall into the area spanned by the pareto-optimal set of solutions as feasible (e.g. Fenicia et al., 2007; Gharari et al., 2013). For brevity, we will
230 hereafter refer to the solution with the minimum Euclidean distance D_E as the "best" solution (Hrachowitz et al., 2014):

$$D_E = \sqrt{\left(1 - E_{NS,Q}\right)^2 + \left(1 - E_{NS,log(Q)}\right)^2} \quad (3)$$

Model uncertainty intervals were constructed from the parameter sets that were retained as feasible using D_E as informal likelihood measure to weight each solution (cf. Freer et al., 1996).

In addition, storage-outflow relationships for the reservoirs (ID9-10; Eq.2) to estimate water release from the associated sub-
235 basins downstream of the reservoirs $UHRB_D$ (ID2) and $UARB_D$ (ID5) were established as ordinary least squares estimates based on inflows from the calibrated upstream sub-basins ($UHRB_U$, ID1; $UARB_U$, ID4), Equation 1 and observations of reservoir water release in the 1970-1975 period. The parameter ranges for all solutions retained as feasible for all calibrated hydrological models and both reservoir routing schemes are given in Table 2. Note that due to physiographic similarity, the uncalibrated model for CHRB (ID3) was run with the same parameter sets as $UHRB_U$ (ID1).

240 The robustness of the calibrated model and its ability to reproduce the time series of daily flow with respect to $E_{NS,Q}$ and $E_{NS,log(Q)}$ in the four calibration sub-basins as well as downstream of the reservoirs was evaluated for the independent 1976-1979 test period, hereafter referred to as "validation period". In addition, the model output was evaluated against monthly time series of flow at SISP (ID8; Table 1; Figure 1) for the entire 1976-2006 study period.

https://doi.org/10.5194/hess-2020-369
Preprint. Discussion started: 24 July 2020


Hydrology and Earth System Sciences
Discussions

4.2 Drought indices

Three previously developed drought indices, based on the general concept of standardized deficits (e.g. Moravec et al., 2019), were used here to isolate the individual influences of different factors on hydrological drought in the HRB. The role of climatic variability and thus meteorological drought was quantified with the Standard Precipitation Index (SPI) as introduced by McKee et al. (1993), which gives information about deficits in atmospheric water supply, and with the Standardized Precipitation Evapotranspiration Index (SPEI; Vicente-Serrano et al., 2010), which describes the interaction of precipitation and energy supply as moisture deficit $D_i = \sum_{i=1}^{T}(P_i - E_{p,i})$ and thus the additional role of atmospheric water demand. In contrast, hydrological drought was quantified with the Streamflow Drought Index (SDI; Nalbantis and Tsakiris, 2009). Differences between SPI and SPEI on the one hand and SDI on the other hand were subsequently used to analyse for potential effects of anthropogenic influences, such as irrigation water abstraction. In a parametric approach, two-parameter Gamma distributions functions were here fitted to precipitation P and flow Q and then mapped to standard normal distributions using equal probability transformations (Edwards & McKee, 1997) to estimate the dimensionless drought indices SPI and SDI, respectively (e.g. Lloyd-Hughes and Saunders, 2002; Nalbantis and Tsakiris, 2009; Mishra et al., 2018), whereas generalized extreme value (GEV) distributions were fitted to moisture deficit D to estimate SPEI for each sub-basin (Stagge et al., 2015). The drought indices can be computed over different time-scales, thus leading to differences in the accumulation of deficits for the corresponding variables (e.g. McKee et al., 1993; Van Loon and Laaha, 2015). Here the drought indices were computed for each month using a time scale of the 12 preceding months as accumulation periods as these were previously found to be the most balanced time scale that give the a balance between short term and long term effects (e.g. Raziei et al., 2009; Gocic et al., 2013; Spinoni et al., 2014). All normalization was carried out relative to the full 1970-2006 study period. Droughts and their associated occurrence probabilities were classified according to the scheme suggested by McKee et al. (1993) as shown in Table 3. Since the drought indices are standardized, the same drought category thresholds were used here for all three of them.

The three drought indices were in the following used to analyse different drought characteristics. It was investigated if drought frequency, duration, severity and intensity exhibit systematic shifts over time or changes in their longitudinal propagation from upstream to downstream over the 37 year study period. Drought frequency D_F [months yr^{-1}] was here defined as the average number of months per year over a specific period in which the respective drought index, i.e. SPI, SPEI or SDI, had a value < 0 (Table 3). Drought duration D_D [months] was defined as the period of consecutive months with drought indices continuously < 0. Drought severity is defined as the total deficit D_{tot} [-] of SPI, SPEI or SDI, respectively, accumulated during all individual continuous drought periods over a specified period and, to allow comparability, normalized by the total number of months N in the time period considered, i.e. $D_S = D_{tot}/N$ [$month^{-1}$]. Drought intensity is expressed as the ratio $D_I = D_{tot}/D_D$ [$month^{-1}$] (Huang et al., 2016).

https://doi.org/10.5194/hess-2020-369
Preprint. Discussion started: 24 July 2020


Hydrology and Earth System Sciences
Discussions

5 Results and discussion

5.1 Drought indices

The hydrological models captured the magnitudes and dynamics of daily flow relatively well when compared to observations available for both, the sub-basins upstream of the reservoirs, i.e. $UHRB_U$ (ID1; Figure 4a) and $UARB_U$ (ID4) as well as for those further downstream, i.e. LARB (ID6) and LHRB (ID7; Figure 4c). For the calibration period the "best" solutions exceeded $E_{NS,Q} > 0.70$ and $E_{NS,log(Q)} > 0.75$ for all five calibrated sub-basins (Table 4). Similar values were found for the validation period with $E_{NS,Q} > 0.70$ and $E_{NS,log(Q)} > 0.75$. The empirical relationships to route flows through the reservoirs during high and low flow periods (Eq.2) were characterized by R^2 =0.80 and 0.57, respectively for the Kajakai Dam Reservoir (ID9) and R^2 =0.92 and 0.76, respectively for the Dahla Dam Reservoir (ID10). The resulting flows at $UHRB_D$ (ID2) and $UARB_D$ (ID5) could be reproduced with $E_{NS,Q} > 0.79$ and $E_{NS,log(Q)} > 0.81$ for the calibration period and comparable performances during the validation period (Figure 4b, Table 4). The ability of these models to reproduce flow upstream, resulted in a robust representation of flow in the Sistan Plain (SISP; ID8) for the entire validation period 1976-2006 without further calibration (Figure 4d, Table 4). Hydrographs of sub-basins not shown in Figure 4 are provided in Figure S1 in the Supplementary Material.

It could be observed that annual peak flows in spring are mostly generated by a combination of snow melt from the high-elevation parts of the HRB, i.e. in sub-basins ID2, 3 and 4, and additional, relatively high-intensity rainfall events (Figure 4). The filling of the two reservoirs attenuates downstream flows, including the annual peaks, throughout spring and into early summer. In turn, the gradual release of water from the reservoirs sustains downstream summer and autumn flows, almost doubling long-term average low flow rates as compared to natural flow conditions (Figures 4, 5), to meet irrigation demand in the downstream Helmand Valley and to satisfy flow requirements Iran under the Iranian-Afghan Helmand River Water Treaty (1973).

Furthermore, the models adequately reproduced the losing character of the downstream sub-basins, including LHRB (ID7) and SISP (ID8). Thus, in this highly water-limited environment these sub-basins do not generate relevant volumes of flow. Rather, most of the precipitation and, in addition, significant volumes of water entering LHRB (ID7) and eventually SISP (ID8) as flow from upstream, eventually evaporate. Besides this, streamflow draining LHRB (ID7) and crossing a hyper-arid desert region is reduced by about 60% before reaching SISP (ID8), as specified by the calibrated loss factor K_L. These streamflow reductions cannot be explained by soil evaporation alone in this essentially vegetation-free environment. It is not implausible to assume that most of these losses are caused by the river losing water as deep-infiltration and recharge of a deep aquifer.

https://doi.org/10.5194/hess-2020-369
Preprint. Discussion started: 24 July 2020


Hydrology and Earth System Sciences
Discussions

5.2 Temporal pattern of drought

5.2.1 SPI

Multiple meteorological drought events in terms of SPI occurred in the HRB throughout the 1970-2006 study period (Figure 6a). An average mean drought frequency across all sub-basins of the HRB of $D_{F,SPI}$ = 6.3 months year^{-1} characterized the 1970-1979 decade. This is slightly higher than in the subsequent two decades during which $D_{F,SPI}$ reached 5.5 and 3.9 months year^{-1}, respectively. The last part of the study period, 2000-2006, experienced more precipitation deficits again, resulting in frequent drought spells with $D_{F,SPI}$ = 8.4 months year^{-1}. A similar pattern was found for drought duration. While the first three decades of the study period experienced mean drought durations across all sub-basins between $D_{D,SPI}$ = 9.2 and 10.6 months, much longer droughts occurred in the 2000-2006 period with $D_{D,SPI}$ = 21.1 months (Figure 6a). Reflecting the above, the mean drought severity and intensity were also more pronounced at the beginning and towards the end of the study period, with lowest mean $D_{S,SPI}$ = -0.9 and $D_{I,SPI}$ = -1.2 month^{-1}, respectively, in the 2000-2006 period, as compared to the highest $D_{S,SPI}$ = -0.2 and $D_{I,SPI}$ = -0.3 month^{-1} in the wetter period between 1980 and 1999. Notwithstanding the fluctuating pattern in these drought descriptors over the study period, pairwise comparisons of the decadal distributions of basin-average annual SPI values using Wilcoxon rank sum tests indicated that there is no significant difference between any of the decadal SPI distributions ($p > 0.05$), as also shown in Figure 7a. Correspondingly, no temporal trends in the time series of annual SPI could be detected based on Mann-Kendall tests (Kendall, 1975) for the HRB or any sub-basin therein ($p > 0.05$; Figure 7b). These results suggest that precipitation and the associated meteorological drought due to precipitation deficit did, in spite of decadal fluctuations, not experience a systematic change in the HRB over the four study decades.

5.2.2 SPEI

The temporal pattern of drought in terms of SPEI, reflecting the combined effects of precipitation water supply and atmospheric water demand, similarly indicate the occurrence of multiple periods of severe drought in all sub-basins throughout the HRB during the 1970-2006 study period (Figure 6b). The temporal fluctuations in SPEI broadly correspond with those in SPI, suggesting that most drought events are largely controlled by water supply and thus precipitation deficits rather than by increased atmospheric water demand in this arid region. More specifically, mean drought frequency across all sub-basins decreased from $D_{F,SPEI}$ = 6.6 months year^{-1} in the 1970-1979 decade to 5.2 and 4.0 months year^{-1}, respectively, in the following two decades. In the last decade of the study period, however, a pronounced increase in drought frequency to $D_{F,SPEI}$ = 8.9 months year^{-1} was observed (Figure 6b). While individual drought events had average durations between $D_{D,SPEI}$ = 8.4 and 12.9 months in the first three decades across all sub-basins, this substantially increased to $D_{D,SPEI}$ = 20.2 months in the multi-year drought in the 2000-2006 decade. Drought severity and intensity remained at relatively modest levels not falling below $D_{S,SPEI}$ = -0.4 and $D_{I,SPEI}$ = -0.6 month^{-1}, respectively, in the 1980-1999 period. In contrast, the first and last decade were characterized by much higher severity and intensity, with the lowest mean $D_{S,SPEI}$ = -1.0 and $D_{I,SPEI}$ = -1.1 month^{-1}, respectively, occurring during the 2000-2006 period. Similar to SPI, Wilcoxon rank sum tests showed that there is

https://doi.org/10.5194/hess-2020-369
Preprint. Discussion started: 24 July 2020


Hydrology and Earth System Sciences
Discussions

mostly no systematic and significant difference between the decadal distributions of basin-average SPEI ($p > 0.05$), with the exception of the 2000-2006 decade, during which SPEI is significantly lower than during the 1990-1999 decade for most sub-basins ($p \leq 0.05$), as shown in Figure 7c. The temporal sequence of a slight SPEI increase during the first three decades followed by a sharp decrease during the multi-year drought in 2000-2006 likewise illustrates that there is no systematic trend in the time series of SPEI in the HRB or any sub-basin therein over the study period ($p > 0.05$; Figure 7d).

5.2.3 SDI

Streamflow drought, as specified by SDI, was quantified based on streamflow estimates as obtained from the best available model solution for each of the eight sub-basins. It could be observed that SDI largely follows the temporal pattern in SPI and SPEI (Figure 6c), respectively, with a relatively low lag time of ≤ 1 month in all sub-basins throughout the HRB, as suggested by a cross-correlation analysis between time series of monthly SPI, SPEI and SDI in the individual sub-basins ($r = 0.66 – 0.91$; $p < 0.05$; not shown). However, it can also be observed that, overall, SDI drought events are less pronounced than SPI and SPEI droughts occurring at around the same time. More specifically it was found that the mean drought frequency across all sub-basins fluctuated between $D_{F,SDI} = 4.7$ and 6.2 months year^{-1}in the first three decades of the study period. In the 2000-2006 decade it experienced a marked increase to $D_{F,SDI} = 9.3$ months year^{-1}. Mean drought duration, in contrast, was with $D_{D,SDI} = 30.3$ months highest in the 1980-1989 decade, albeit associated with low drought intensities and thus very mild drought events. Similarly long durations ($D_{D,SDI} = 28.7$ months), yet with markedly higher intensities occurred during the 2000-2006 period. In the other two decades the mean $D_{D,SDI}$ did not exceed 16 months. Closely reflecting the pattern of SPI and SPEI, mean drought severity and intensity across all sub-basins were most pronounced in the first and last decades with both $D_{S,SDI}$ and $D_{I,SDI}$ reaching a minimum value of -1.0 month^{-1}in the 2000-2006 period. During the wetter decades in-between $D_{S,SDI}$ and $D_{I,SDI}$ did not decrease below values of -0.2 and -0.5 month^{-1}, respectively.

Following a pairwise comparison of all decadal basin-average SDI distributions, the slight, yet statistically insignificant increase of the decadal SPI and SPEI distributions ($p > 0.05$; Figures 7a,c) from 1970-1999 could not be observed in SDI, which remained rather stable during the first three decades (Figure 7e). In contrast, the decrease of SPEI in the last decade is reflected in correspondingly lower basin-average SDI in the 2000-2006 period ($p \leq 0.05$; Figure 7e). However, the time series of basin-average SDI did not exhibit a significant trend ($p > 0.05$; Figure 7f).

5.3 Spatial pattern, synchronicity and propagation of drought

5.3.1 SPI

In most years of the study period meteorological drought, as specified by SPI, exhibits considerable spatial coherence and synchronicity throughout the HRB (Figure 6a). In other words, at any given time, the entire HRB experiences similar relative precipitation deficits (or surpluses), with a median $r = 0.97$ ($p < 0.05$) as obtained from a Spearman rank correlation between the time series of SPI across all sub-basins. Regional differences in SPI remain limited to parts in the central HRB, i.e.

https://doi.org/10.5194/hess-2020-369
Preprint. Discussion started: 24 July 2020


Hydrology and Earth System Sciences
Discussions

CHRB (ID3) and LARB (ID6, Figure 6a). In contrast to the remainder of the HRB, these two sub-basins are characterized by multiple periods that are, in relative terms, more humid, such as in 1974 or 1982, but also by periods that are, in comparison, considerably drier, such as 1987 or 1994. The elevated degree of spatial coherence and synchronicity in SPI on the scale of the HRB is further illustrated by the comparison of the upstream and downstream decadal SPI distributions (Figure 8a). No significant differences ($p > 0.05$) between the SPI distribution of the six most upstream sub-basins (ID1-ID6) and the SPI distribution of the two most downstream sub-basins, LHRB (ID7) and SISP (ID8), could be found in any of the four decades during the study period. To provide some more explicit spatial context, the spatial distribution of SPI at the resolution of the individual model grid cells for four selected years is shown in Figure 9a-d. Compared to the SPI aggregated at the scales of the individual sub-basins (Figure 6a), this more detailed picture corroborates the level of large-scale spatial coherence, in spite of somewhat increased local variations in SPI (Figure 9a-d). A rather rare exception is the year 1987, which was characterized by a substantial North-South gradient in SPI spatial variations and whose extent is largely masked by the aggregation of SPI to the sub-basin scale in Figure 6a.

5.3.2 SPEI

While SPEI is widely coherent (median $r = 0.94$, $p < 0.05$) and spatially broadly follows the pattern of SPI throughout large parts of the HRB, it can also be observed that inter-annual differences in atmospheric water demand, here estimated based on E_P, lead to modest, yet contrasting effects (Figure 6b). For some sub-basins and time periods characterized by comparably cool temperatures, water deficits are attenuated and SPEI thus remains higher than SPI (e.g. $UARB_U$-ID4 in 1986 or LARB-ID6 in 1989). For other sub-basins and warmer time periods increased atmospheric water demand reinforces water deficits (e.g. CHRB-ID3 in 1981). As shown in Figure 8a, the distributions of SPEI closely reflect the distributions of SPI in the first decade of the study period. In the following 1980-1989 decade as well as in the 2000-2006 decade SPEI is lower than SPI, potentially indicating the role of E_P in intensifying water deficits in these periods. In contrast, the opposite effect can be observed during the 1990-1999 decade, where rather low E_P had a moderating effect, leading to higher values of SPEI than SPI. Although these effects occur across the entire HRB, water deficits in terms of SPEI are considerably more sensitive to fluctuations in atmospheric water demand and the differences between SPEI and SPI are thus more pronounced in the downstream parts of the HRB (Figure 8a). In particular, SPEI in the hyper-arid SISP (ID8; Figure 6b) is characterized by a low degree of coherence and synchronicity compared to upstream SPEI, exhibiting both, markedly more severe water deficits (e.g. 1973, 1984 or 2003) but also more pronounced water surpluses (e.g. 1986, 1996 or 2005). Notwithstanding these varying effects of E_P on water deficits and thus on the differences between SPEI and SPI, no systematic temporal trend of E_P reinforcing/moderating water deficits could be detected.

5.3.3 SDI

Hydrological drought in terms of SDI during the study period exhibited a lower degree of spatial coherence and synchronicity (Figure 6c) across the HRB. This is reflected by a lower median $r = 0.85$ ($p < 0.05$) from pairwise Spearman

https://doi.org/10.5194/hess-2020-369
Preprint. Discussion started: 24 July 2020


Hydrology and Earth System Sciences
Discussions

Rank correlations between the individual time series of SDI across all sub-basins. The spatially and temporally more heterogeneous mosaic of SDI, however, allows a few insights. The data suggest that both reservoirs, at Kajakai dam and Dahla dam, respectively, have effects on the propagation of hydrological drought. This can be seen in the differences in SDI between the sub-basins upstream ($UHRB_U$-ID1; $UARB_U$-ID4) and the associated sub-basins downstream of the dams ($UHRB_D$-ID2; $UARB_D$-ID5) in Figure 6c. In the early phase of the study period, the reservoirs had some moderating effects on the propagation of hydrological droughts, most notably for the 1977 (both dams) and 1971 (Dahla dam) droughts. The median SDI in the 1970-1979 decade was ~0.2 higher downstream than upstream of both reservoirs ($p < 0.05$). However, over the following decades, both reservoirs largely lost their drought attenuating functions and the reservoir at Dahla dam may have even contributed to amplifying the 1999-2002 drought downstream of the dam, with a median SDI over that period being ~0.18 ($p < 0.05$) lower at the downstream $UARB_D$ (ID5) than the upstream $UARB_U$ (ID4).

While the distribution of SDI broadly follows the distributions of SPI and SPEI in the upstream part of the HRB (ID1-ID6), downstream hydrological drought is characterized by rather distinct dynamics (ID7-ID8; Figure 8a). In contrast to the basin-average time series of SDI (Figure 7f), SDI in the two downstream sub-basins exhibit clear negative trends over the four decades of the study period ($p \leq 0.05$; not shown). In addition, the data suggest that for the 1970-1979 decade the median downstream SDI ~ 0.2 is significantly higher ($p < 0.05$) than SPI, SPEI and upstream SDI, which are all characterized by a median of about -0.1 (Figure 8a). As also shown by the individual SDI distributions of all sub-basins in Figure 8b, hydrological drought is considerably attenuated and the relative river water deficits reduced compared to upstream parts of the HRB during that period. However, throughout the following two decades, the downstream moderation of hydrological drought weakens, i.e. the distributions of downstream SDI more closely reflect those of SPI, SPEI and upstream SDI (Figure 8b). This pattern then eventually fully inverts into a downstream drought amplification in the 2000-2006 decade, during which the median downstream SDI = -1.5 is significantly lower ($p < 0.05$) than not only the median upstream SDI = -0.9 but also than SPI and SPEI (Figures 8a,b). This shift from downstream drought moderation to drought amplification can be seen clearly for the four selected years in Figure 9e-h. In spite of dry meteorological conditions throughout the HRB in 1977 (Figure 9a) and severe hydrological drought in the North of the HRB, no drought occurred in the South of the study region (Figure 9e). In 1987, similarly, the increasing precipitation deficits from upstream to downstream (Figure 9b) were buffered and not reflected in the North-South gradient of SDI, indicating the wettest conditions in the most downstream part of the HRB (Figure 9f). The extreme opposite of the above two examples occurred in the last decade of the study period. In both years, 2002 and 2003, respectively, spatially relatively coherent precipitation pattern across the entire HRB (Figure 9c-d) led to severe hydrological drought in the most downstream parts of the HRB in particular at SISP (ID8; Figure 9g-h). This is particularly striking for the rather wet year 2003, in which SDI in the upstream sub-basins reflected the generally wet conditions of that year, while further downstream river water deficits developed, gradually amplifying to a severe drought at SISP (ID8). Further analysis of the time series of the difference between upstream (ID1-ID6) and downstream (ID7-8) SDI (i.e. ΔSDI) shows the inversion from a negative to a positive ΔSDI over the 37 years of the study period occurred gradually and, according to a Mann-Kendall test, following a significant trend ($p < 0.05$), while the differences in SPI remain stable

https://doi.org/10.5194/hess-2020-369
Preprint. Discussion started: 24 July 2020


Hydrology and Earth System Sciences
Discussions

over time (Figure 8c). This suggests that it may not be implausible to assume that the inversion of downstream hydrological drought moderation in the 1970-1979 decade into drought amplification in the 2000-2006 decade was, at least partly, an effect of systematic, longer-term shifts in the system rather than a short-term, synchronous occurrence of multiple drought-amplifying hydro-meteorological conditions, such as sustained high precipitation deficits and high atmospheric water demand. Such short-term influences would be likely to manifest themselves in a more erratic temporal evolution of ΔSDI.

5.4 Drought drivers and process attribution

The above drought indices provide only limited information to identify dominant drivers of droughts. To gain more understanding of the spatio-temporal pattern of hydrological drought and to eventually attribute droughts to physical processes estimates of the absolute magnitudes of multiple modelled hydrological fluxes, as obtained from the best available model solution for each sub-basin, are in the following analysed.

With a long-term mean annual precipitation of ~250 mm y^{-1} in the HRB, the overall magnitudes of streamflow deficits, and thus of hydrological droughts, are clearly dominated by fluctuations in precipitation anomalies (Figure 10a), with a mean absolute anomaly of around ±50mm y^{-1} for the entire HRB or ~ 20% of the long-term mean water balance. In contrast, anomalies in total evaporation E_A (here: $E_A = E_I + E_T + I_D$) exhibit much lower variability in this arid environment, with a mean absolute anomaly of about ±20 mm y^{-1}. As water supply is the limiting factor for evaporation, the highest rates of E_A occur in the wettest years (Figure 10b). Conversely, E_A has proportionally less impact on streamflow in dry years. In general it can be seen that precipitation anomalies of ~ -50 – -100 mm y^{-1} lead to streamflow anomalies of ~ -20 – -30 mm y^{-1} (Figure 10c).

The modelled data suggest that during drought years, the reservoir at Kajakai Dam released slightly less water ($UHRB_D$-ID2) than it received as inflow ($UHRB_U$-ID1), as shown in Figure 4. The mean difference between drought period inflow to and outflow from the reservoir remained stable at ΔQ ~ 0.9 mm y^{-1} throughout the four decades of the study period. This implies that there is no evidence that the reservoir neither moderated nor significantly amplified downstream propagation of streamflow deficits, underlining the very minor role of this reservoir for drought pattern. In contrast, the modelled flow estimates for the reservoir at Dahla Dam suggest that this reservoir had some moderation effect on downstream flow deficits and thus drought propagation in the first decade of the study period. On average, the reservoir outflow ($UARB_D$-ID5) during drought periods in that decade exceeded the inflow ($UARB_U$-ID4) by ΔQ ~ 1.1 mm y^{-1} (Supplementary Figure S1). However, this difference gradually decreased over time and eventually converged towards zero in the 2000-2006 period. In spite of uncertainties arising from data and the modelling process, this nevertheless indicates the possibility that the Dahla Dam reservoir has lost its, albeit very minor, drought-moderating function over the study period.

For further analysis the HRB was separated into an upper and a lower basin. The upper basin comprises $UHRB_D$ (ID2), CHRB (ID3) and LARB (ID3), which together drain into the lower basin, here defined as LHRB (ID7) only and thus for clarity of presentation excluding SISP (ID8). As illustrated by Figure 10, and consistent with the spatial analysis of drought indices in Section 5.3, the general pattern of anomalies correspond well between the upper and the lower basin, suggesting a

https://doi.org/10.5194/hess-2020-369
Preprint. Discussion started: 24 July 2020


Hydrology and Earth System Sciences
Discussions

considerable level of spatial coherence and drought synchronicity. However, reflecting the evolution of ΔSDI (Figure 8c), a subtle but gradual shift in the difference between streamflow anomalies of the upper and lower basins from, on average, -9.4 mm y^{-1} in the 1970-1979 decade to 5.5 mm y^{-1} in the 2000-2006 period is evident (Figure 10c). Thus, while anomalies were less negative/more positive, therefore indicating proportionally "more" water, in the lower than in the upper basin at the beginning of the study period, the opposite was true at the end of the study period. This entails that in the first decade of the study period streamflow deficits from the upper basin were to some degree attenuated in the lower basin. This effect was gradually reduced and finally completely inversed in the last decade of the study period. During the 2000-2006 period streamflow anomalies from the upper basin were systematically amplified in the lower basin. The absence of a similar systematic shift in the difference of precipitation anomalies between the upper and the lower basin (Figure 10a) strongly suggests alternative reasons for the above effects.

The analysis of the relative contributions of different water fluxes from the upper and lower basins, respectively, as well as their evolution over time as estimated from the models allowed some more detailed insights into these pattern. The combined water balance of all three sub-basins of the upper basin for the 1970-1979 period (Figure 11a) shows that of the mean annual precipitation P ~ 202 mm y^{-1} of the upper basin, 28% drained away as streamflow (Q ~ 56 mm y^{-1}) and the remainder of 72% was released as combined evaporative fluxes (E_A ~ 146 mm y^{-1}). While transpiration (E_T ~ 130 mm y^{-1}) and interception evaporation (E_I ~ 9 mm y^{-1}) played a role throughout the entire upper basin, irrigation demand (I_D ~ 7mm y^{-1}) was limited to the agriculturally used areas of the LARB (ID6) sub-basin and thus only accounted for ~ 4% of the water balance of the upper basin. The flow partitioning of the lower basin for the same period exhibited considerably different pattern. It can be seen in Figure 11a that of the available water in the lower basin (~ 97 mm y^{-1}), i.e. precipitation over the LHRB (ID7) sub-basin plus the combined inflow from the upper basin, 51% (Q ~ 49 mm y^{-1}) is drained as streamflow and 49% are released as evaporative flux (E_A ~48 mm y^{-1}). In comparison to the upper basin, irrigation demand accounts with ~ 14% for a substantially larger fraction of the water balance in the lower basin (I_D ~ 13 mm y^{-1}).

During the 2000-2006 period (Figure 11b), the upper basin received slightly less precipitation (P ~ 179 mm y^{-1}) than in the 1970-1979 period. However, the relative contributions of the different fluxes remained rather stable over time. The fraction of water drained as streamflow slightly decreased to 25% (Q ~ 44 mm y^{-1}), while the fraction of evaporative fluxes correspondingly increased to 75 % (E_A ~ 135 mm y^{-1}) of the water balance of the upper basin with similar increases for all three evaporative components (Figure 11b). In contrast, substantial shifts in the flux partitioning can be observed for the lower basin (Figure 11b). In spite of a reduction of available water to ~ 71 mm y^{-1} in the 2000-2006 period, the evaporative release (E_A ~ 49 mm y^{-1}) reached the same level as in the 1970-1979 decade. As illustrated by Figure 11b, the high levels of evaporative release were sustained by significant absolute and relative increases of irrigation demand to I_D ~ 23 mm y^{-1} or 32% of the water available in the lower basin (or ~10% of the water balance of the entire HRB). This in turn resulted in a reduction of streamflow to Q ~ 22 mm y^{-1}, equivalent to a reduction from 51% of the water balance in the 1970-1979 decade to 31% in the 2000-2006 decade. The increases of I_D and the corresponding decreases in Q are directly related to increases in agricultural area over the study period (Figure 2). It is therefore plausible to assume that the inversion of the function of the

https://doi.org/10.5194/hess-2020-369
Preprint. Discussion started: 24 July 2020


Hydrology and Earth System Sciences
Discussions

lower basin from moderation to amplification of flow deficits and the associated droughts is largely a consequence of the extension the cultivated area and the related increased water demand for successful crop cultivation.

Overall, the magnitudes of flow deficits and the associated hydrological droughts are largely driven by precipitation deficits across the HRB. The two reservoirs in the HRB had a very minor effects on the propagation of flow deficits, with levels not exceeding 0.5% of the water balance of the HRB in the study period. In contrast, the increase of agricultural area, mostly in LHRB (ID7), led to an increase of the basin-wide irrigation water demand (i.e. from LARB-ID6 and LHRB-ID7) from ~ 7% to ~ 12% of the water balance of the HRB. While at the scale of the entire HRB this remains of minor relevance for flow deficits, and thus hydrological drought, it led throughout the study period to a continuous change in the downstream propagation of flow deficits from moderation to amplification. This illustrates that flow deficits and droughts in the HRB clearly reflect the dynamic interplay between temporally varying regional differences in hydro-meteorological variables together with subtle and temporally varying effects linked to direct human intervention.

5.5 Uncertainties, unresolved questions and limitations

All above results are necessarily conditional on a range of uncertainties and choices made during the modelling process (Beven, 2006; Hrachowitz and Clark, 2017). This is in particular relevant in the HRB, where detailed and reliable data are scarce. It entails further, that although the results of this study are largely consistent with the available data, the data themselves may inaccurately reflect reality. In addition, where of sufficient quality, the available data may not have sufficient detail to accurately represent the underlying mechanistic processes and/or changes thereof over time in a model. Two major sources of uncertainty, due to the lack of detailed and high-quality data need to be explicitly highlighted for this study. First, the routing of flows through the two reservoirs in the HRB was estimated with a simple empirical relationship (Eq.2) based on data from the 1970-1979 period, under the assumption that this relationship did not change over time. In reality, reservoir operation rules may have changed over the study period, yet this cannot be clarified with the available data. However, even if such changes occurred, their impact is likely limited, as model evaluation at SISP (ID8) showed that adequate model performances were achieved throughout the entire study period (Table 3, Figure 4).

A second unresolved issue is the observed and modelled considerable reduction of stream flow between LHRB (ID7) and SISP (ID8). The loss of ~ 60% of streamflow as the river crosses the desert region between Afghanistan and Iran cannot be explained by evaporation. In the model it was represented by an unspecified loss factor K_L. A clearer mechanistic interpretation was not warranted by the available data. Potential explanations include deep infiltration losses of stream water to deep aquifers of unknown location and extent. Another cause that cannot be completely ruled out is a potentially very low quality of the available streamflow data either at LHRB (ID7), at SISP (ID8) or at both of them.

We explicitly reiterate here that although this modelling study allowed robust insights into pattern of drought characteristics, including changes in downstream drought propagation over time, the absolute magnitudes of variables reported herein remain, for the above reasons, highly uncertain. These magnitudes should therefore, under no circumstances and without

https://doi.org/10.5194/hess-2020-369
Preprint. Discussion started: 24 July 2020


Hydrology and Earth System Sciences
Discussions

more detailed data and understanding of the underlying processes, be used for direct policy advice in this arid environment where the transboundary nature of the HRB makes water scarcity a highly sensitive issue.

6 Conclusions

In a combined data analysis and modelling study in the transboundary Helmand River Basin (HRB) we analysed spatial patterns of drought and changes therein over the 1970-2006 study period, based on the drought indices SPI, SPEI and SDI, as well as on absolute water deficits. The results provide some evidence that:

(1) Drought characteristics varied throughout the study period. In general, the 2000-2006 and partly the 1970-1979 periods were drier than the decades in between. Depending on the drought index, mean drought duration reached $D_D \sim 20 – 30$ months and mean drought intensity $D_I \sim -1.0$ month^{-1} in these drier periods, as compared to $D_D \sim 8 – 16$ months and $D_I \sim -0.3 – -0.6$ in the 1980-1999 period.

(2) The basin-average decadal distributions of the drought indices largely exhibited no statistically significant differences, with the exception of significantly lower SPEI and SDI in 2000-2006 compared to the preceding decades. In addition, no systematic trend over time was detected for any of the basin-average drought indices.

(3) All three drought indices exhibit considerable spatial coherence and synchronicity across the HRB throughout the study period. This indicates that in most cases droughts similarly affect the entire HRB with little regional or local defences.

(4) The overall magnitudes of streamflow drought in the HRB are consistently controlled by precipitation deficits, while the effects of the two reservoirs as well as water abstraction for irrigation on flow deficits remain minor during drought years, accounting for only 0.5 % and ~10%, respectively, of the water balance of the HRB.

(5) The downstream parts of the HRB moderated the further propagation of streamflow deficits and the associated droughts in the early decades of the study period. This drought moderation function of the lower basin was gradually and systematically inverted by the end of the study period, when the lower basin eventually amplified the downstream propagation of flow deficits and droughts.

(6) The shift from drought moderation to drought amplification in the lower basin is very likely a consequence of agricultural activity and the associated increased irrigation water demand in spite of being only a minor fraction of the water balance.

Overall the results of this study illustrate that flow deficits and the associated droughts in the HRB clearly reflect the dynamic interplay between temporally varying regional differences in hydro-meteorological variables together with subtle and temporally varying effects linked to direct human intervention.

https://doi.org/10.5194/hess-2020-369
Preprint. Discussion started: 24 July 2020


Hydrology and Earth System Sciences
Discussions

References

Ahmad, M. and Wasiq, M.: Water resources development in Northern Afghanistan and its implications for Amu Darya Basin (English), World Bank working paper series, Washington, D.C., World Bank Group. 36, 66 pp., 2004.

Ahmadalipour, A., Moradkhani, H., and Demirel, M. C.: A comparative assessment of projected meteorological and hydrological droughts: Elucidating the role of temperature, J. Hydrol., 553, 785-797, https://doi.org/10.1016/j.jhydrol.2017.08.047, 2017.

Ajami, N. K., Gupta, H., Wagener, T., and Sorooshian, S.: Calibration of a semi-distributed hydrologic model for streamflow estimation along a river system, J. Hydrol., 298, 112–135, https://doi.org/10.1016/j.jhydrol.2004.03.033, 2004.

Alami, M. M. and Tayfor, G.: Meteorological Drought Analysis by Different Methods in Helmand River Basin, Afghanistan, Int. J. Sci. Eng. Res., 8, 738-744, https://doi.org/10.14299/ijser.2018.02.004, 2018.

Al-Faraj, F. A. M. and Scholz, M.: Assessment of temporal hydrologic anomalies coupled with drought impact for a transboundary river flow regime: The Diyala watershed case study, J. Hydrol., 517, 64-73, https://doi.org/10.1016/j.jhydrol.2014.05.021, 2014.

Allen, R., Pereira, L., Raes, D., and Smith, M.: Crop evapotranspiration - Guidelines for computing crop water requirements, FAO Irrigation and drainage paper No. 56, 300 pp., 1998.

Arnold, J., Srinivasan, R., Muttiah, R., and Williams, J.: Large area hydrologic modeling and assessment part I: model development, J. Am. Water Resour. Assoc., 34, 73–89, https://doi.org/10.1111/j.1752-1688.1998.tb05961.x, 1998.

Ashraf Vaghefi, S., Abbaspour, N., Kamali, B., and Abbaspour, K. C.: A toolkit for climate change analysis and pattern recognition for extreme weather conditions – Case study: California-Baja California Peninsula, Environ. Modell. Software, 96, 181-198, https://doi.org/10.1016/j.envsoft.2017.06.033, 2017.

Beven, K. J.: A manifesto for the equifinality thesis, J. Hydrol., 320, 18–36, https://doi.org/10.1016/j.jhydrol.2005.07.007, 2006.

Beven, K.: On hypothesis testing in hydrology, Hydrol. Processes, 15, 1655-1657, https://doi.org/10.1002/hyp.436, 2001.

Bouaziz, L., Weerts, A., Schellekens, J., Sprokkereef, E., Stam, J., Savenije, H., and Hrachowitz, M.: Redressing the balance: quantifying net intercatchment groundwater flows, Hydrol. Earth Syst. Sci., 22, 6415–6434, https://doi.org/10.5194/hess-22-6415-2018, 2018.

Coerver, H. M., Rutten, M. M., and van de Giesen, N, C.: Deduction of reservoir operating rules for application in global hydrological models, Hydrol. Earth Syst. Sci., 22, 831–851, https://doi.org/10.5194/hess-22-831-2018, 2018.

Ebrahimzadeh, I. and Esmaelnejad, M.: Climate change and the role of recent droughts on agricultural economy of Sistan, Romanian Review of Regional Studies., IX, 11-22, 2013.

Edwards, D.C. and McKee, T.B.: Characteristics of 20th Century Drought in the United States at Multiple Time Scales, Department of Atmospheric Science, Colorado State University, Fort Collins, Climatology Report 97-2, 1997.

Euser, T., Hrachowitz, M., Winsemius, H., and Savenije, H.: The effect of forcing and landscape distribution on performance and consistency of model structures, Hydrol. Processes, 29, 3727–3743, https://doi.org/10.1002/hyp.10445, 2015.

Euser, T., Winsemius, H. C., Hrachowitz, M., Fenicia, F., Uhlenbrook, S., and Savenije, H. H. G.: A framework to assess the realism of model structures using hydrological signatures, Hydrol. Earth Syst. Sci., 17, 1893–1912, https://doi.org/10.5194/hess-17-1893-2013, 2013.

Fenicia, F., Kavetski, D., and Savenije, H. H. G.: Elements of a flexible approach for conceptual hydrological modeling: 1. Motivation and theoretical development, Water Resour. Res., 47, 1-13, https://doi.org/10.1029/2010WR010174, 2011.

Fenicia, F., Savenije, H. H. G., Matgen, P., and Pfister, L.: A comparison of alternative multiobjective calibration strategies for hydrological modeling, Water Resour. Res., 43, 1-16, https://doi.org/10.1029/2006WR005098, 2007.

Fenicia, F., Savenije, H. H. G., Matgen, P., and Pfister, L.: Understanding catchment behaviour through stepwise model concept improvement, Water Resour. Res., 44, 1-13, https://doi.org/10.1029/2006WR005563, 2008.

Freer, J., Beven, K., and Ambroise, B.: Bayesian Estimation of Uncertainty in Runoff Prediction and the Value of Data: An Application of the GLUE Approach, Water Resour. Res., 32, 2161-2173, https://doi.org/10.1029/95WR03723, 1996.

Gao, H., Ding, Y., Zhao, Q., Hrachowitz, M., and Savenije, H. H. G.: The importance of aspect for modelling the hydrological response in a glacier catchment in Central Asia, Hydrol. Processes, 31, 2842–2859, https://doi.org/10.1002/hyp.11224, 2017.

Gao, H., Hrachowitz, M., Fenicia, F., Gharari, S., and Savenije, H. H. G.: Testing the realism of a topography-driven model (FLEX-Topo) in the nested catchments of the Upper Heihe, China, Hydrol. Earth Syst. Sci., 18, 1895–1915, https://doi.org/10.5194/hess-18-1895-2014, 2014.

Geng, S., Devries, F., and Supit, I.: A simple method for generating daily rainfall data, Agr. Forest Meteorol., 36, 363-376, https://doi.org/10.1016/0168-1923(86)90014-6, 1986.

Gharari, S., Hrachowitz, M., Fenicia, F., and Savenije, H. H. G.: An approach to identify time consistent model parameters: sub-period calibration, Hydrol. Earth Syst. Sci., 17, 149–161, https://doi.org/10.5194/hess-17-149-2013, 2013.

Gharari, S., Shafiei, M., Hrachowitz, M., Kumar, R., Fenicia, F., Gupta, H. V., and Savenije, H. H. G.: A constraint-based search algorithm for parameter identification of environmental models, Hydrol. Earth Syst. Sci., 18, 4861–4870, https://doi.org/10.5194/hess-18-4861-2014, 2014.

Gocic, M. and Trajkovic, S.: Analysis of precipitation and drought data in Serbia over the period 1980–2010, J. Hydrol., 494, 32-42, https://doi.org/10.1016/j.jhydrol.2013.04.044, 2013.

Goes, B. J. M., Howarth, S. E., Wardlaw, R. B., Hancock, I. R., and Parajuli, U. N.: Integrated water resources management in an insecure river basin: a case study of Helmand River Basin, Afghanistan, Int. J. Water Resour. Dev., 32, 3-25, http://dx.doi.org/10.1080/07900627.2015.1012661, 2016.

Gupta, H. V., Sorooshia, S., and Yapo, P. O.: Toward improved calibration of hydrologic models: Multiple and noncommensurable measures of information, Water Resour. Res., 34, 751-763, https://doi.org/10.1029/97WR03495, 1998.

https://doi.org/10.5194/hess-2020-369
Preprint. Discussion started: 24 July 2020

Haddeland, I., Heike, J., Biemans, H., Eisner, S., Flörke, M., Kanasaki, N., Konzmann, M., Ludwig, F., Masaki, Y., Schewe, J., Stacke, t., Tessler, Z. D., Wada, Y., and Wisser, D.: Global water resources affected by human interventions and climate change, PNAS, 111, 3251-3256, https://doi.org/10.1073/pnas.1222475110, 2014.

Hajihosseini, H., Hajihosseini, M., Morid, S., Delavar, M., and Booij, M. J.: Hydrological Assessment of the 1973 Treatyon the Transboundary Helmand River, Using the SWAT Model and a Global Climate Database, Water Resour. Manag., 30, 4681–4694, https://doi.org/10.1007/s11269-016-1447-y, 2016.

Hajihosseini, M., Hajihosseini, H., Morid, S., Delavar, M., and Booij, M. J.: Impacts of land use changes and climate variability on transboundary Hirmand River using SWAT, J. Water Clim. Change [Preprint], https://doi.org/10.2166/wcc.2019.100, 18 October 2019.

Hanasaki, N., Kanae, S., and Oki, T.: A reservoir operation scheme for global river routing models, J. Hydrol., 327, 22-41, https://doi.org/10.1016/j.jhydrol.2005.11.011, 2006.

Harris, I., Jones, P. D. Osborn, T. J., and Lister, D. H.: Updated high-resolution grids of monthly climatic observations – the CRU TS3.10 Dataset, Int. J. Climatol., 34, 623-642, https://doi.org/10.1002/joc.3711, 2014.

Hrachowitz, M. and Clark, M. P.: HESS Opinions: The complementary merits of competing modelling philosophies in hydrology, Hydrol. Earth Syst. Sci., 21, 3953–3973, https://doi.org/10.5194/hess-21-3953-2017, 2017.

Hrachowitz, M., Fovet, O., Ruiz, L., Euser, T., Gharari, S., Nijzink, R., Freer, J., Sanenije, H. H. G., and Gascuel-Odoux, C.: Process consistency in models: The importance of system signatures, expert knowledge, and process complexity, Water Resour. Res., 50, 7445–7469, https://doi.org/10.1002/2014WR015484, 2014.

Huang, S., Huang, Q., Chang, J., and Leng, G.: Linkages between hydrological drought, climate indices and human activities: a case study in the Columbia River basin, Int. J. Climatol., 36, 280-290, https://doi.org/10.1002/joc.4344, 2016.

Hulsman, P., Winsemius, H. C., Michailovsky, C., Savenije, H. H., & Hrachowitz, M. (2020). Using altimetry observations combined with GRACE to select parameter sets of a hydrological model in data scarce regions. Hydrology and Earth System Sciences, 24, 3331-3359.

Jiao, Y. and Yuan, X.: More severe hydrological drought events emerge at different warming levels over the Wudinghe watershed in northern China, Hydrol. Earth Syst. Sci., 23, 621–635, https://doi.org/10.5194/hess-23-621-2019, 2019.

Konz, M. and Seibert, J.: On the value of glacier mass balances for hydrological model calibration, J. Hydrol., 385, 238-246, https://doi.org/10.1016/j.jhydrol.2010.02.025, 2010.

Kubiak-Wójcicka, K. and Bąk, B.: Monitoring of meteorological and hydrological droughts in the Vistula basin (Poland), Environ. Monit. Assess., 190, 691, https://doi.org/10.1007/s10661-018-7058-8, 2018.

LIoyd-Hughes, B. and Saunders, M. A.: A drought climatology for Europe, Int. J. Climatol., 22, 1571-1592, https://doi.org/10.1002/joc.846, 2002.

Liu, Y. Ren, L., Zhu, Y., Yang, X., Yuan, F., Jiang, S., and Ma, M.: Evolution of Hydrological Drought in Human Disturbed Areas: A Case Study in the Laohahe Catchment, Northern China, Adv. Meteorol., 2016, 1-12, https://doi.org/10.1155/2016/5102568, 2016.

McKee, T. B., Doesken, N. J., and Kleist, J.: The relationship of drought frequency and duration to time scales, in: Eighth Conference on Applied Climatology, Anaheim, California, 17-22 January 1993, 1993.

Mishra, A. K. and Singh, V. p.: A review of drought concepts, J. Hydrol., 391, 202-216, https://doi.org/10.1016/j.jhydrol.2010.07.012, 2010.

Mishra, V., Shah, R., Azhar, S., Shah, H., Modi, P., and Kumar, R.: Reconstruction of droughts in India using multiple land-surface models (1951–2015), Hydrol. Earth Syst. Sci., 22, 2269–2284, https://doi.org/10.5194/hess-22-2269-2018, 2018.

Miyan, M. A.: Droughts in Asian Least Developed Countries: Vulnerability and sustainability, Weather Clim. Extremes, 7, 8-23, https://doi.org/10.1016/j.wace.2014.06.003, 2015.

Moravec, V., Markonis, Y., Rakovec, O., Kumar, R., and Hanel, M.: A 250-Year European Drought Inventory Derived From Ensemble Hydrologic Modeling, Geophys, Res. Lett., 46, 5909-5917, https://doi.org/10.1029/2019GL082783, 2019.

Mostbauer, K., Kaitna, R., Prenner, D., and Hrachowitz, M.: The temporally varying roles of rainfall, snowmelt and soil moisture for debris flow initiation in a snow-dominated system, Hydrol. Earth Syst. Sci., 22, 3493–3513, https://doi.org/10.5194/hess-22-3493-2018, 2018.

Nalbantis, I. and Tsakiris, G.: Assessment of Hydrological Drought Revisited, Water Resour. Manage., 23, 881–897, https://doi.org/10.1007/s11269-008-9305-1, 2009.

Nash, J. E. and Sutcliffe, J. V.: River flow forecasting through conceptual models: part I —A discussion of principles, J. Hydrol., 10, 282–290, https://doi.org/10.1016/0022-1694(70)90255-6, 1970.

Nijzink, R. C., Almeida, S., Pechlivanidis, I. G., Capell, R., Gustafssons, D., Arheimer, B., Parajka, J., Freer, J., Han, D., Wagener, T., van Nooijen, R. R. P., Savenije, H. H. G., and Hrachowitz, M.: Constraining Conceptual Hydrological Models With Multiple Information Sources, Water Resour. Res., 54, 1-31, https://doi.org/10.1029/2017WR021895, 2018.

Parajka, J. and Blöschl, G.: Spatio-temporal combination of MODIS images – potential for snow cover mapping, Water Resour. Res., 44, 1-13, https://doi.org/10.1029/2007WR006204, 2008.

Pathak, A. A. and Dodamani, C. B. M.: Comparison of two hydrological drought indices, Perspect. Sci., 8, 626-628, https://doi.org/10.1016/j.pisc.2016.06.039, 2016.

Piqué, G., Batalla, R. J., and Sabater, S.: Hydrological characterization of dammed rivers in the NW Mediterranean region, Hydrol. Processes, 30, 1691–1707, https://doi.org/10.1002/hyp.10728, 2016.

Prenner, D., Kaitna, R., Mostbauer, K., and Hrachowitz, M.: The Value of Using Multiple Hydro-meteorological Variables to Predict Temporal Debris Flow Susceptibility in an Alpine Environment, Water Resour. Res., 54, 6822-6843, https://doi.org/10.1029/2018WR022985, 2018.

Raziei, T., Saghafian, B., Paulo, A. A. Pereira, L. S., and Bordi, I.: Spatial patterns and temporal variability of drought in western Iran, Water Resour. Manage., 23, 439–455, https://doi.org/10.1007/s11269-008-9282-4, 2009.

Schuol, J. and Abbaspour, K. C.: Calibration and uncertainty issues of a hydrological model (SWAT) applied to West Africa, Adv. Geosci., 9, 137–143, https://doi.org/10.5194/adgeo-9-137-2006, 2006.

https://doi.org/10.5194/hess-2020-369
Preprint. Discussion started: 24 July 2020


Hydrology and Earth System Sciences
Discussions

Schuol, J., Abbaspour, K. C., Yang, H., Srinivasan, R., and Zehnder, A. J. B.: Modeling blue and green water availability in Africa, Water Resour. Res., 44, 1-18, https://doi.org/10.1029/2007WR006609, 2008.

Spinoni, J., Naumann, G., Carrao, H., Barbosa, P., and Vogt, J.: World drought frequency, duration, and severity for 1951–2010, Int. J. Climatol., 34, 2792–2804, https://doi.org/10.1002/joc.3875, 2014.

Stagge, J.H., Tallaksen, L.M., Gudmundsson, L., van Loon, A.F., and Stahl, K.: Candidate distributions for climatological drought indices (SPI and SPEI), Int. J. Climatol., 35, 4027-4040, http://dx.doi.org/10.1002/joc.4267, 2015.

Trambauer, P., Maskey, S., Werner, M., Pappenberger, F., van Beek, L. P. H., and Uhlenbrook, S.: Identification and simulation of space–time variability of past hydrological drought events in the Limpopo River basin, southern Africa, Hydrol. Earth Syst. Sci., 18, 2925–2942, https://doi.org/10.5194/hess-18-2925-2014, 2014.

United Nation Office on Drugs and Crime (UNODC), Afghanistan Opium Survey, Government of Afghanistan, Ministry of Counter Narcotics, Kabul, 150 pp., 2006.

Van Beek, E., Bozorgi, B., Vekerdy, Z., and Meijer, K.: Limits to agricultural growth in the Sistan Closed Inland Delta, Iran, Irrig. Drain. Syst., 22, 131-143, https://doi.org/10.1007/s10795-008-9045-7, 2008.

Van Huijgevoort, M. H. J., van Lanen, H. A. J., Teuling, A. J., and Uijlenhoet, R.: Identification of changes in hydrological drought characteristics from a multi-GCM driven ensemble constrained by observed discharge, J. Hydrol., 512, 421-434, https://doi.org/10.1016/j.jhydrol.2014.02.060, 2014.

Van Lanen, H. A. J., Wanders, N., Tallaksen, L. M., and Van Loon, A. F.: Hydrological drought across the world: impact of climate and physical catchment structure, Hydrol. Earth Syst. Sci., 17, 1715–1732, https://doi.org/10.5194/hess-17-1715-2013, 2013.

Van Loon, A. F. and Laaha, G.: Hydrological drought severity explained by climate and catchment characteristics, J. Hydrol., 526, 3-14, https://doi.org/10.1016/j.jhydrol.2014.10.059, 2015.

Van Loon, A. F., Rangecroft, S., Coxon, G., Breña Naranjo, J. A., Van Ogtrop, F., and Van Lanen, H. A. J.: Using paired catchments to quantify the human influence on hydrological droughts, Hydrol. Earth Syst. Sci., 23, 1725–1739, https://doi.org/10.5194/hess-23-1725-2019, 2019.

Vicente-Serrano, S. M., Beguería, S., and López-Moreno, J. I.: A Multiscalar Drought Index Sensitive to Global Warming: The Standardized Precipitation Evapotranspiration Index, J. Climate, 23, 1696–1718, https://doi.org/10.1175/2009JCLI2909.1, 2010.

Vicente-Serrano, S. M., López-Moreno, J. I., Beguería, S., and Lorenzo-Lacruz, J.: Accurate Computation of a Streamflow Drought Index, J. Hydrol. Eng., 17, 318-332, https://doi.org/10.1061/(ASCE)HE.1943-5584.0000433, 2012.

Vining, K. C. and Vecchia, A. V.: Water-Balance Simulations of Runoff and Reservoir Storage for the Upper Helmand Watershed and Kajakai Reservoir, Central Afghanistan, U.S. Agency for International Development, Sci. Invest. Rep., 2007–5148, 24 pp., 2007.

https://doi.org/10.5194/hess-2020-369
Preprint. Discussion started: 24 July 2020

725 Wada, Y., Reager, J. T., Chao, B. F., Wang, J., Lo, M. H., Song, C., Li, Y., and Gardner, A. S.: Recent changes in land water storage and its contribution to sea level variations, Surv. Geophys., 38, 131-152, https://doi.org/10.1007/s10712-016-9399-6, 2016.

Wardlaw, R., Goes, B., Parajuli, U., and Hancock, I.: Helmand River Basin Master Plan, Phase 3, Water Resources Modelling for Helmand River Basin, Ministry of Energy and Water, Kabul, Technical Report., 3, 251 pp., 2013.

730 Weng, B., Zhang, P., and Li, S.: Drought risk assessment in China with different spatial scales, Arabian J. Geosci., 8, 10193-10202, https://doi.org/10.1007/s12517-015-1938-9 , 2015.

Whitney, J. W.: Geology, Water, and Wind in the Lower Helmand Basin, Southern Afghanistan, U.S. Agency for International Development, Sci. Invest. Rep., 2006–5182, 50 pp., 2006.

Wisser, D., Fekete, B. M., Vörösmarty, C. J., and Schumann, A. H.: Reconstructing 20th century global hydrography: a
735 contribution to the Global Terrestrial Network- Hydrology (GTN-H), Hydrol. Earth Syst. Sci., 14, 1–24, https://doi.org/10.5194/hess-14-1-2010, 2010.

Wu, J., Chen, X., Yao, H., Gao, L., Chen, Y., and Liu, M.: Non-linear relationship of hydrological drought responding to meteorological drought and impact of a large reservoir, J. Hydrol., 551, 495-507, https://doi.org/10.1016/j.jhydrol.2017.06.029, 2017.

740 Yassin, F., Razavi, S., Elshamy, M., Davison, B., Sapriza-Azuri, G., and Wheater, H.: Representation and improved parameterization of reservoir operation in hydrological and land-surface models, Hydrol. Earth Syst. Sci., 23, 3735–3764, https://doi.org/10.5194/hess-23-3735-2019, 2019.

Zhang, D., Liu, X., Liu, C., and Bai, P.: Responses of runoff to climatic variation and human activities in the Fenhe River, China, Stochastic Environ. Res. Risk Assess., 27, 1293-1301, https://doi.org/10.1007/s00477-012-0665-y, 2013.

745

750

https://doi.org/10.5194/hess-2020-369
Preprint. Discussion started: 24 July 2020

Hydrology and Earth System Sciences
Discussions
Open Access
EGU

755 **Table 1**. Summary of sub-basins and reservoirs in the Helmand River Basin. UHRB, CHRB and LHRB denote the Upper, Central and Lower Helmand River Basins, respectively, UARB and LARB are the Upper and Lower Arghandab River Basins, respectively and SISP is the Sistan Plain. The subscripts U and D are inflows into the reservoir upstream of the dams and outflows from the reservoirs downstream of the dams, respectively.

Location ID	Sub-basin Symbol	Station name	Latitude (°)	Longitude (°)	Average Elevation (m)	Precipitation (mmy^{-1})	Discharge (mmy^{-1})	Aridity Index (-)	Observation Period (daily/monthly)	Reservoir Storage (10^6 m^3)
1	$UHRB_U$	Dehraout – Kajakai Dam inflow	32.42	65.28	2865	300	130	0.29	1970–1979 (d)	----
2	$UHRB_D$	Kajakai Dam outflow	32.19	65.06	2798	300	111	0.29	1970–1979 (d)	----
3	CHRB	-	-	-	1994	204	-	0.13	-	
4	$UARB_U$	Upper Arghandab – Dahla Dam inflow	31.50	65.52	2830	254	91	0.22	1970–1979 (d)	----
5	$UARB_D$	Dahla Dam outflow	31.57	66.02	2776	254	88	0.22	1970–1979 (d)	----
6	LARB	Qala-i-Bust	31.30	64.23	2509	225	32	0.13	1970–1980 (d)	----
7	LHRB	Char Burjak	30.17	62.02	2610	229	43	0.16	1970–1979 (d)	----
8	SISP	Sistan	30.49	61.46	2584	250	15	0.16	1970–2006 (m)	----
9		Kajakai Dam Reservoir	32.19	65.10	963	----	----		----	1800
10		Dahla Dam Reservoir	31.52	65.54	1070	----	----		----	450

760

https://doi.org/10.5194/hess-2020-369
Preprint. Discussion started: 24 July 2020

Hydrology and Earth System Sciences
Discussions

Table 2: Uniform prior and posterior distributions of model parameters for the calibrated models. The posterior column distributions show the parameter values of the best available parameter set as well as the 5/95th percentile of feasible solutions (in brackets). Note that loss factor K_L had negligible influence and was thus set to 0 for the models of ID6 and ID7 to keep to the principle of model parsimony.

ID	Sub-basin symbols	Parameter	Prior distribution	Posterior distribution
1	$UHRB_U$	I_{max} [mm]	0-2	0.13 (0.11-0.55)
		C_e [-]	0.2-1	0.44 (0.36-0.57)
		S_{umax} [mm]	40-800	250 (112-550)
		β [-]	0.2-3	1.08 (0.68-1.55)
		P_{max} [mm d^{-1}]	0.009-1	0.67 (0.65-0.70)
		T_{lag} [d]	2-7	3.12 (3.00-3.84)
		K_f [d^{-1}]	0.01-0.1	0.07 (0.06-0.08)
		K_s [d^{-1}]	0.0009-0.01	0.001 (0.001-0.002)
		T_{th} [°C]	-2.5 – 2.5	-1.12 (-1.42 -0.69)
		F_{dd} [mm °C^{-1} d^{-1}]	0-3	0.38 (0.27-0.51)
4	$UARB_U$	I_{max} [mm]	0-2	0.45 (0.10-0.83)
		C_e [-]	0.2-1	0.84 (0.41-0.84)
		S_{umax} [mm]	40-800	200 (100-430)
		β [-]	0.2-3	1.73 (0.93-2.27)
		P_{max} [mm d^{-1}]	0.009-1	0.47 (0.15-0.47)
		T_{lag} [d]	2-7	2.41 (2.00-3.01)
		K_f [d^{-1}]	0.01-0.1	0.07 (0.03-0.08)
		K_s [d^{-1}]	0.0009-0.01	0.001 (0.001-0.003)
		T_{th} [°C]	-2.5 – 2.5	-1.35 (-1.50 -1.14)
		F_{dd} [mm °C^{-1} d^{-1}]	0-3	0.85 (0.39-1.99)
6	LARB	I_{max} [mm]	0.1-3	1.66 (0.97-2.15)
		C_e [-]	0.1-1	0.23 (0.18-0.33)
		S_{umax} [mm]	40-600	455 (200-515)
		β [-]	0.1-3.00	2.76 (1.56-2.82)
		P_{max} [mm d^{-1}]	0.01-0.1	0.04 (0.03-0.05)
		T_{lag} [d]	2-7	3.45 (2.12-4.18)
		K_f [d^{-1}]	0.01-1.00	0.02 (0.01-0.02)
		K_s [d^{-1}]	0.0009-0.01	0.009 (0.008-0.01)
		K_L [-]	0.00	0.00 (0.00-0.00)
7	LHRB	I_{max} [mm]	0.1-3	1.58 (0.27-1.85)
		C_e [-]	0.1-1	0.19 (0.11-0.35)
		S_{umax} [mm]	40-600	515 (220-585)
		β [-]	0.1-3.00	2.81 (1.86-2.88)
		P_{max} (mm/day)	0.01-0.1	0.03 (0.02-0.05)
		T_{lag} [d]	3-10	6.61 (3.42-7.12)
		K_f [d^{-1}]	0.01-1.00	0.03 (0.02-0.05)
		K_s [d^{-1}]	0.0009-0.01	0.009 (0.005-0.01)
		K_L [-]	0.00	0.00 (0.00-0.00)
8	SISP	I_{max} [mm]	0.1-3	1.58 (0.27-1.85)
		C_e [-]	0.1-1	0.19 (0.11-0.35)
		S_{umax} [mm]	40-600	515 (220-585)
		β [-]	0.1-3.00	2.81 (1.86-2.88)
		P_{max} [mm d^{-1}]	0.01-0.1	0.03 (0.02-0.05)
		T_{lag} [d]	3-10	6.61 (3.42-7.12)
		K_f [d^{-1}]	0.01-1.00	0.03 (0.02-0.05)
		K_s [d^{-1}]	0.0009-0.01	0.009 (0.005-0.01)

https://doi.org/10.5194/hess-2020-369
Preprint. Discussion started: 24 July 2020

Hydrology and Earth System Sciences
Discussions

		K_L [-]	0-1	0.34 (0.33 – 0.36)
9	$UHRB_D$	a_h [d^{-1}]	-	0.27 (0.13-0.40)
		b_h [-]	-	0.64 (0.50-0.77)
		c_h [mm d^{-1}]	-	-173 (-332- -15)
		a_l [d^{-1}]	-	0.13 (0.09-0.17)
		c_l [mm d^{-1}]	-	217 (173-262)
10	$UARB_D$	a_h [d^{-1}]	-	0.21 (0.11-0.31)
		b_h [-]	-	0.86 (0.79-0.93)
		c_h [mm d^{-1}]	-	-58 (-84- -32)
		a_l [d^{-1}]	-	0.26 (0.11-0.42)
		c_l [mm d^{-1}]	-	25 (17-33)

https://doi.org/10.5194/hess-2020-369
Preprint. Discussion started: 24 July 2020


Hydrology and Earth System Sciences
Discussions

Table 3. Classification of standardized drought indices DI used in this study (SPI, SPEI and SDI).

795

Classification	DI [-]	Probability [-]
No drought	DI > 0	0.501
Mild drought	-1 ≤ DI < 0	0.341
Moderate drought	-1.5 ≤ DI < -1	0.092
Severe drought	-2 ≤ DI < -1.5	0.044
Extreme drought	DI < -2	0.023

https://doi.org/10.5194/hess-2020-369
Preprint. Discussion started: 24 July 2020

Hydrology and Earth System Sciences
Discussions

Table 4. Model performance metrics for calibration and validation in all study sub-basins. The values include the best performing model as well as the range of all solutions retained as feasible (in brackets)

Location ID	Sub-basin Symbol	Calibration period (1971 – 1975)		Validation period (1976–1979)	
		$E_{NS,Q}$	$E_{NS,log(Q)}$	$E_{NS,Q}$	$E_{NS,log(Q)}$
1	$UHRB_U$	0.82 (0.82-0.83)	0.91 (0.90-0.91)	0.80 (0.79-0.80)	0.86 (0.86-0.87)
2	$UHRB_D$	0.79 (0.78-0.80)	0.81 (0.79-0.82)	0.79 (0.79-0.80)	0.85(0.84-0.86)
4	$UARB_U$	0.83 (0.83-0.84)	0.85 (0.85-0.86)	0.73 (0.72-0.73)	0.78 (0.78-0.89)
5	$UARB_D$	0.89 (0.88-0.90)	0.92 (0.91-0.92)	0.74 (0.74-0.75)	0.80 (0.79-0.81)
6	LARB	0.70 (0.69-0.71)	0.73 (0.71-0.74)	0.81 (0.80-0.83)	0.83 (0.81-0.86)
7	LHRB	0.82 (0.81-0.83)	0.85 (0.83-0.86)	0.84 (0.82-0.86)	0.88 (0.86-0.91)
		(1971 – 1975)		(1976 – 2006)	
8	SISP	0.88 (0.86-0.89)	0.89 (0.87-0.89)	0.73 (0.68-0.74)	0.75 (0.74-0.77)

https://doi.org/10.5194/hess-2020-369
Preprint. Discussion started: 24 July 2020

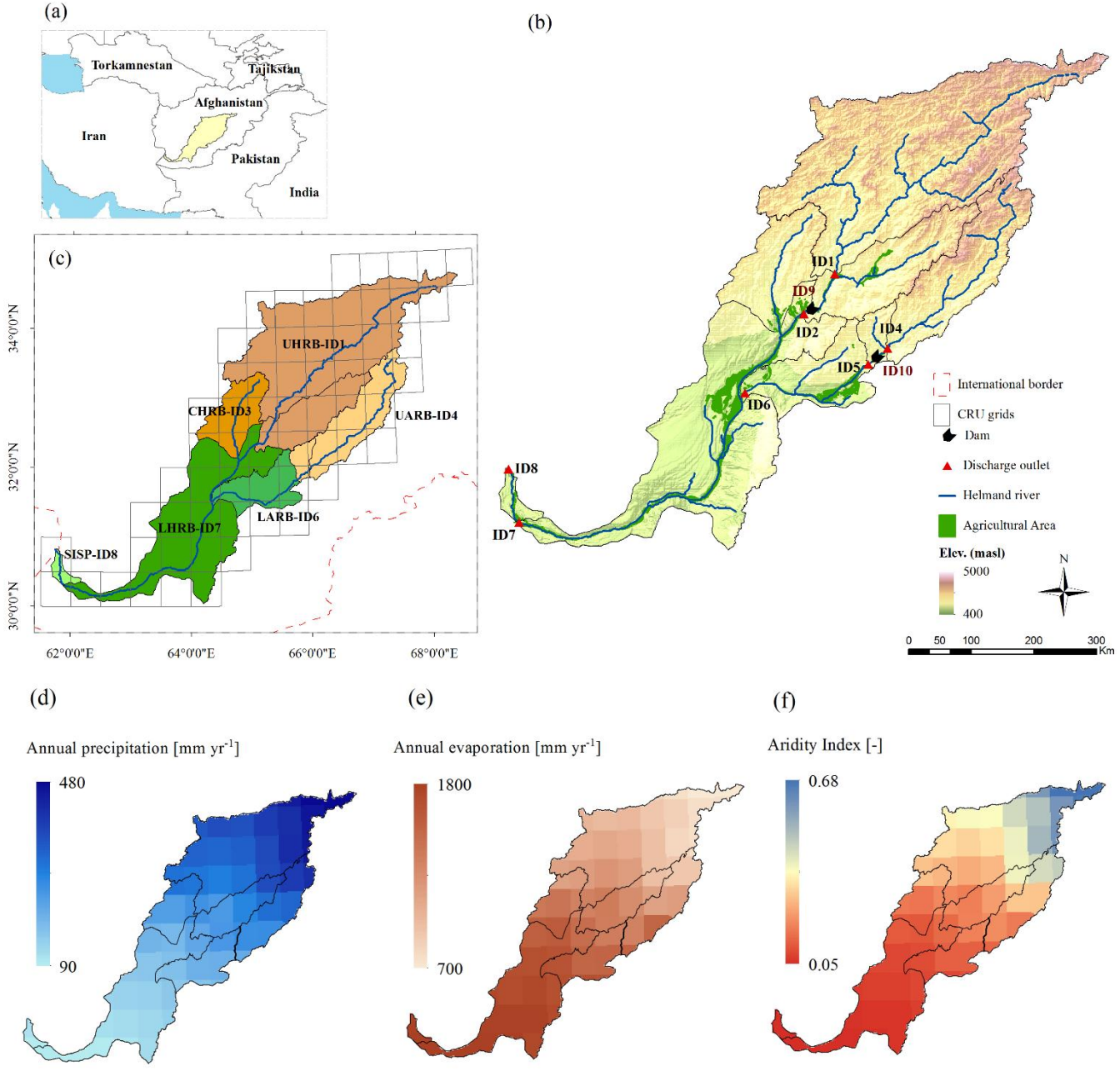

Figure 1. (a) The location of Helmand River Basin (HRB) in central Afghanistan, (b) elevation map of the HRB, also indicating the sub-basin boundaries, the locations of the sub-basin outlets and the agriculturally used area (as of 2006), (c) outline of the sub-basins analysed in this study, including the grid cells of CRU precipitation data used, (d) long-term mean annual precipitation P [mm y^{-1}], (e) long-term mean annual potential evaporation E_P [mm y^{-1}] and (f) the aridity index I_A= P/E_P [-]

https://doi.org/10.5194/hess-2020-369
Preprint. Discussion started: 24 July 2020

Hydrology and Earth System Sciences
Discussions
Open Access
EGU

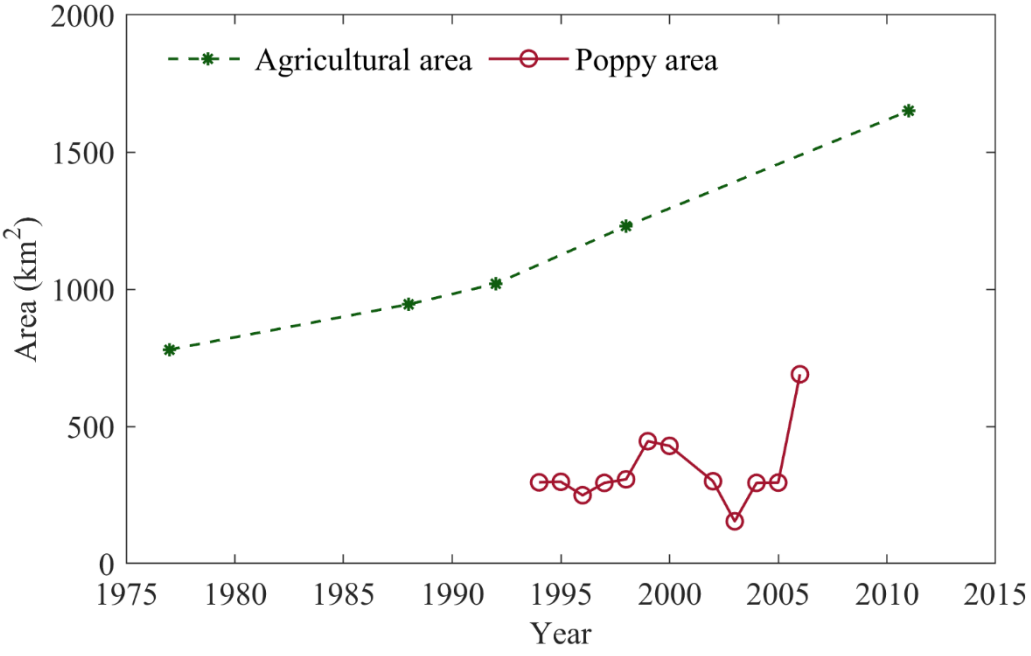

Figure 2. Evolution of total agricultural area in the HRB (1976-2011) and Poppy cultivated area thereof (1994-2006).

https://doi.org/10.5194/hess-2020-369
Preprint. Discussion started: 24 July 2020

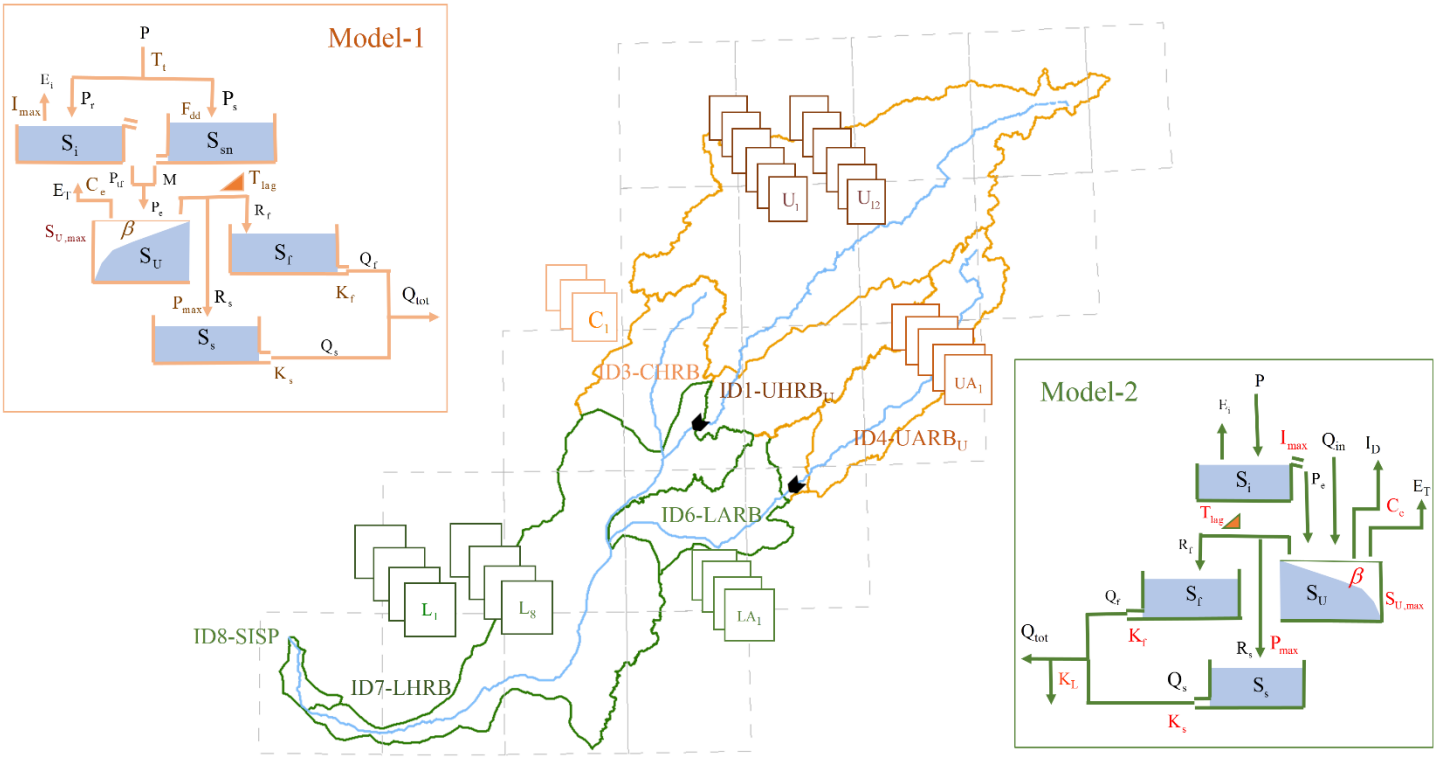

Figure 3. The distributed model structure consisting of parallel components (the structure of Model-1 used for UHRB, CHRB and UARB, Model-2 is used in LHRB, LARB and SISP) and 32 units of CRU grid cell, representing one subbasin each, characterized by an individual parameter set. Variables: P total precipitation [mm d^{-1}], P_s snowfall [mm d^{-1}], P_r rainfall [mm d^{-1}], M snowmelt [mm d^{-1}], P_{tf} throughfall [mm d^{-1}], P_e effective precipitation [mm d^{-1}], E_T transpiration [mm d^{-1}], E_i interception evaporation [mm d^{-1}], R_f recharge of fast reservoir [mm d^{-1}], R_s recharge of slow reservoir [mm d^{-1}], I_D irrigation demand for LHRB and LARB, respectively., $Q_{in} = Q_{UHRB_U} + Q_{LARB} + Q_{CHRB}$ [mm d^{-1}], Q_f runoff from fast reservoir [mm d^{-1}], Q_s runoff from slow reservoir [mm d^{-1}], Q_{tot} = total runoff [mm d^{-1}], S_{sn} storage in snow reservoir [mm], S_i storage in interception reservoir [mm], S_U storage in unsaturated reservoir [mm], S_f storage in fast reservoir [mm], S_s storage in slow reservoir [mm]. Parameters: T_t threshold temperature [℃], F_{dd} melt factor [mm ℃$^{-1}$ d^{-1}], I_{max} interception capacity [mm], $S_{U,max}$ storage capacity in unsaturated reservoir [mm], β shape parameter [-],P_{max} percolation capacity [mm d^{-1}], Ce runoff generation coefficient [-], K_f storage coefficient of fast reservoir [d^{-1}], K_s storage coefficient of slow reservoir [d^{-1}], K_L loss factor [-] and, T_{lag} lag time [d].

https://doi.org/10.5194/hess-2020-369
Preprint. Discussion started: 24 July 2020

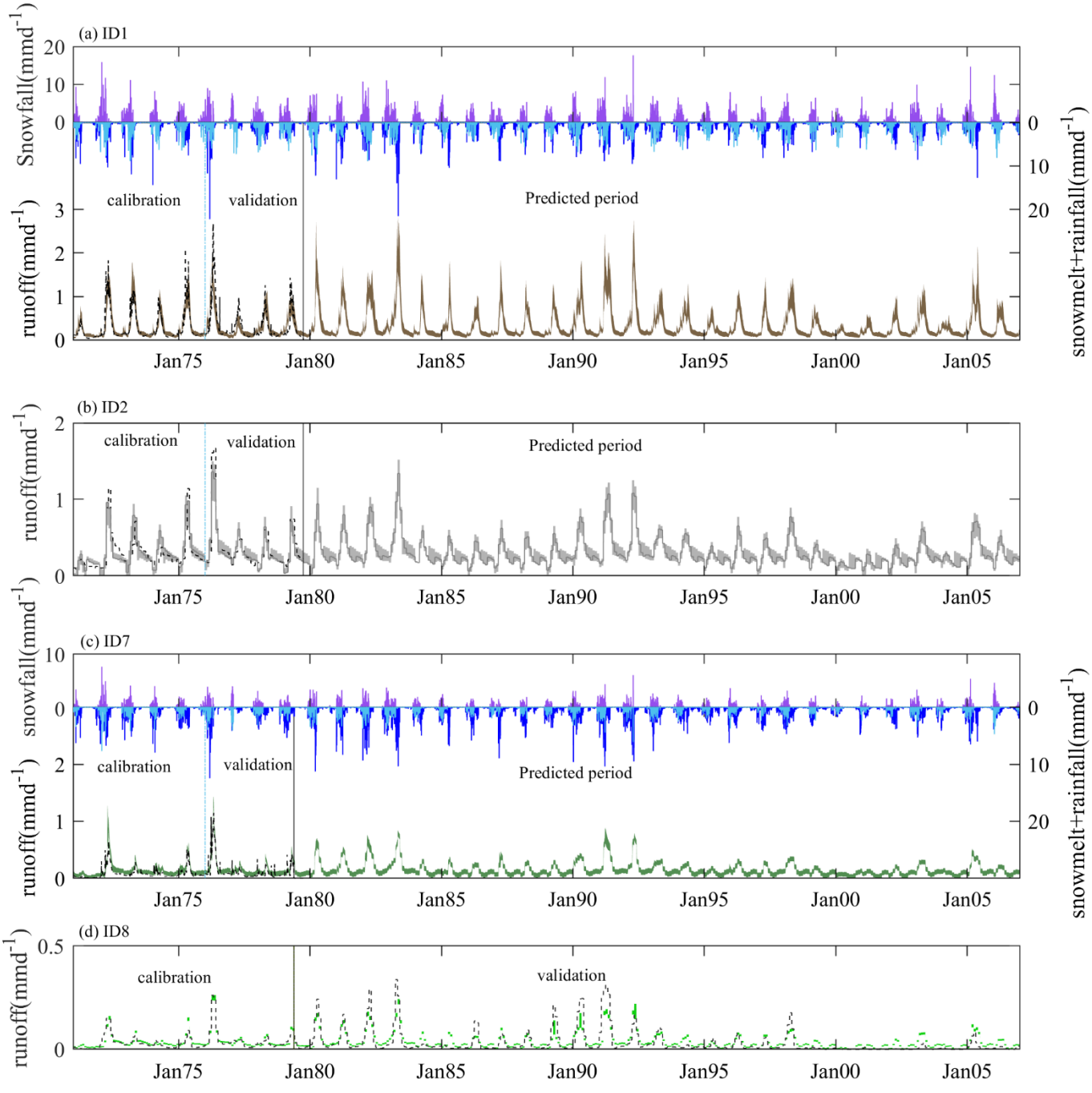

Figure 4. Precipitation and streamflow in $UHRB_U$ (ID1), $UHRB_D$ (ID2), LHRB (ID7), and SISP (ID8). The purple bars show the modelled snowfall P_S [mm d^{-1}], the dark blue bars the modelled snowmelt M [mm d^{-1}] and the light blue bars the modelled rainfall P_R [mm d^{-1}]. The dashed black lines indicate the observed runoff and the shaded areas the uncertainty ranges of modelled runoff during calibration, validation and prediction periods

https://doi.org/10.5194/hess-2020-369
Preprint. Discussion started: 24 July 2020

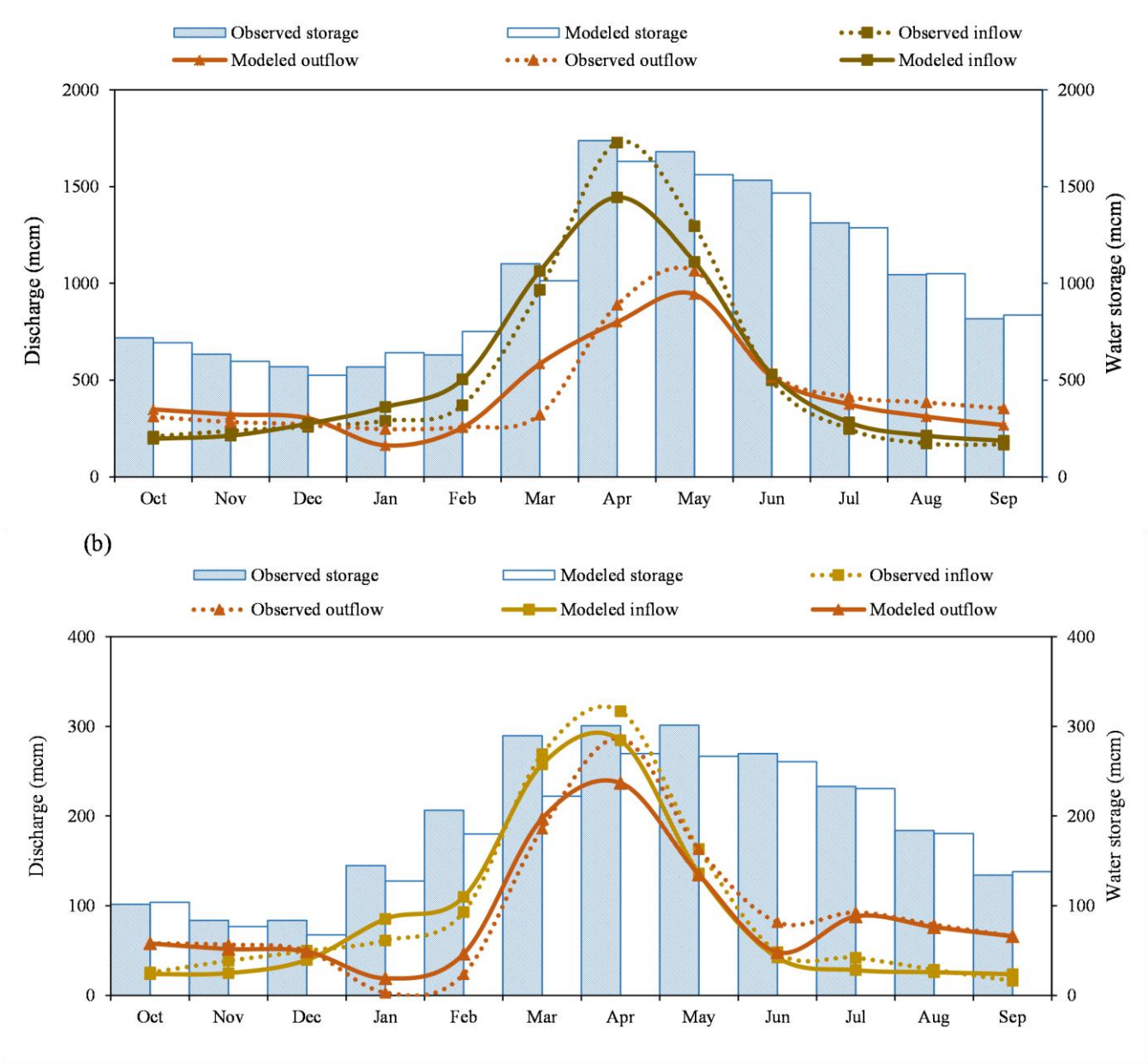

Figure 5. Mean observed and modeled inflow, outflow, and storage volume at (a) the Kajakai and (b) Dahla Dam reservoirs during the 1970–1979 period

865

https://doi.org/10.5194/hess-2020-369
Preprint. Discussion started: 24 July 2020

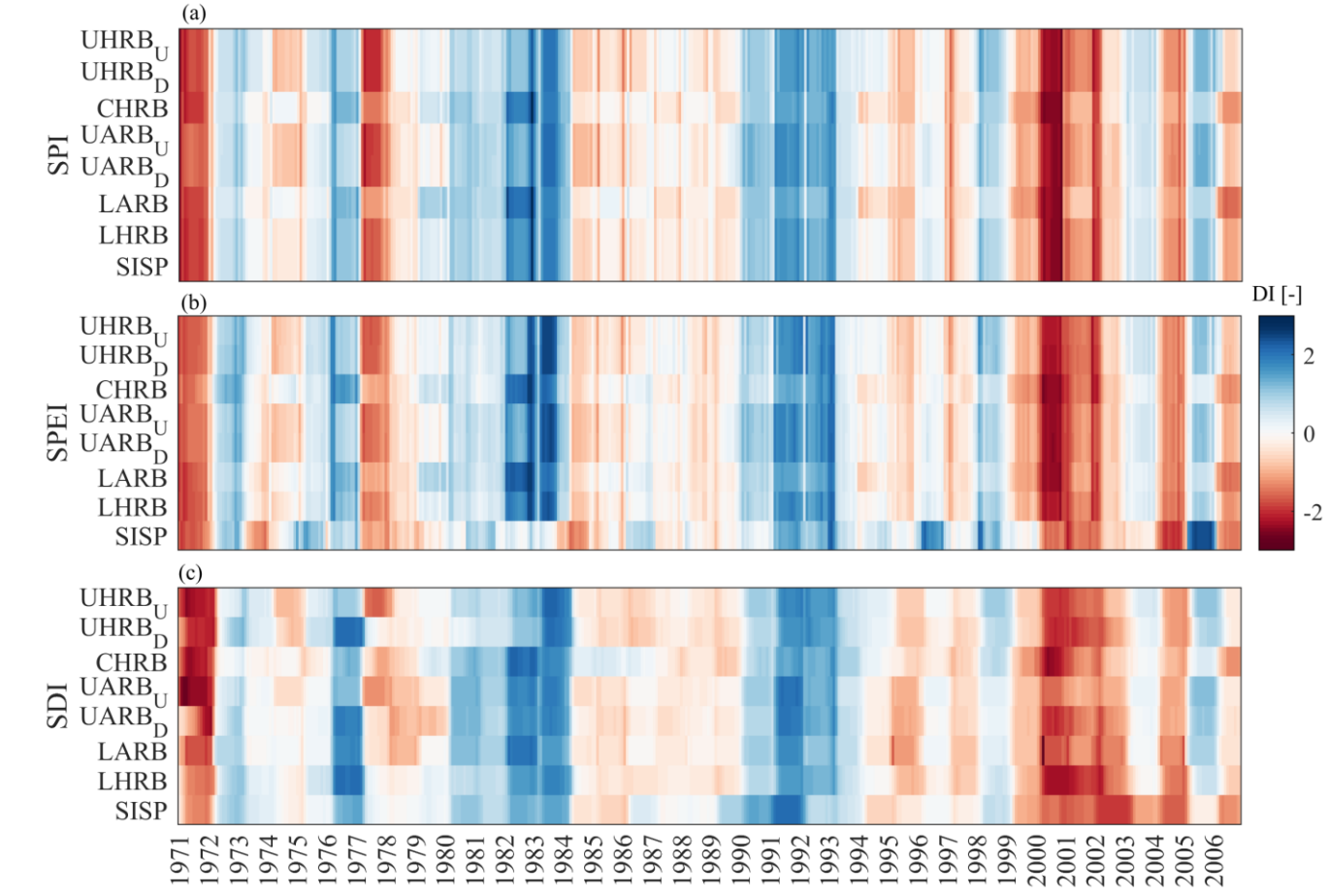

Figure 6. Time series of monthly drought indices (based on 12 months accumulation time) SPI, SPEI and SDI for the sub-basins ID1 – ID8 for the 1970 – 2006 study period

https://doi.org/10.5194/hess-2020-369
Preprint. Discussion started: 24 July 2020

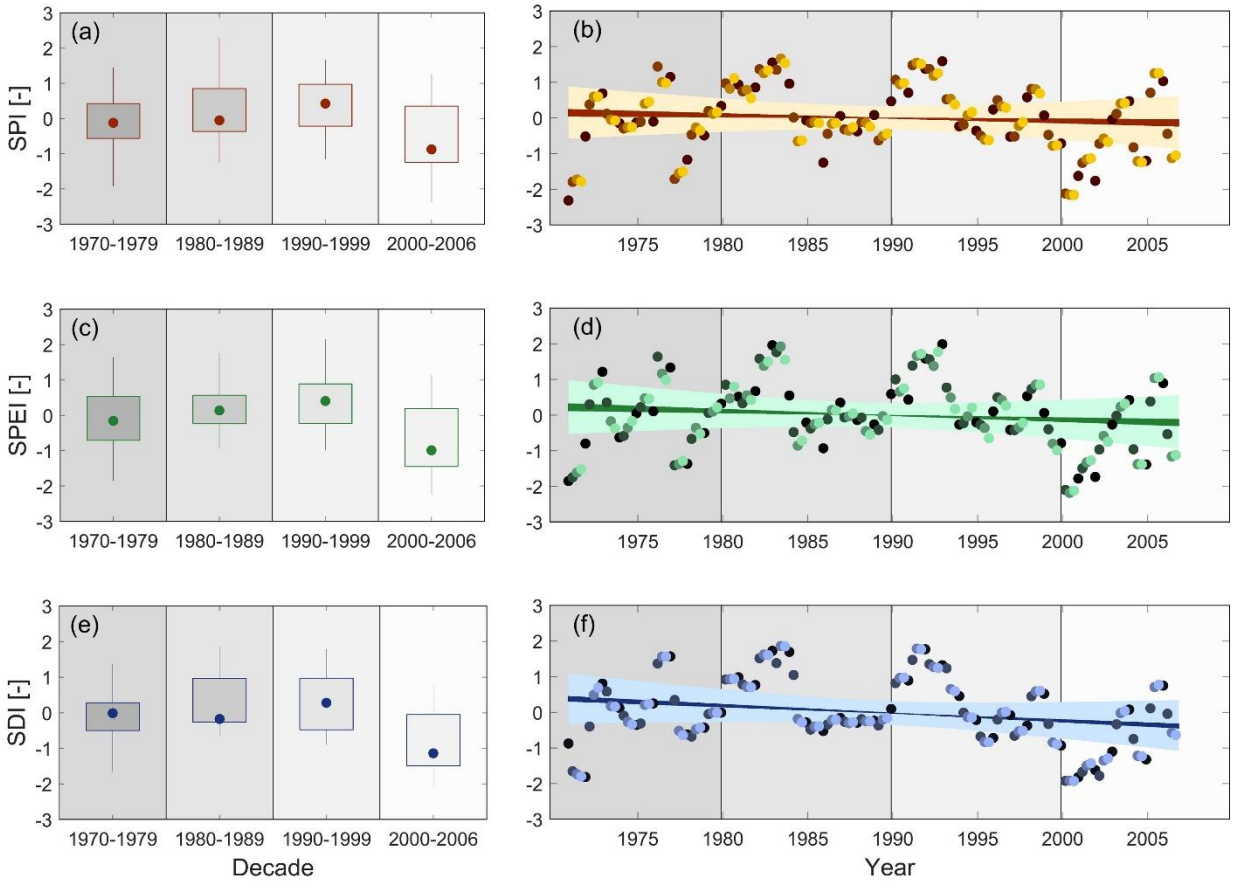

Figure 7. Decadal distributions and time series of mean basin (a)-(b) SPI, (c)-(d) SPEI and (e)-(f) SDI over the study period. The dots in the box plots indicate the median values and the whiskers the 5/95th percentiles. The dark to light shaded dots in the time series plots indicate the monthly drought indices (based on 12 months accumulation time) for all months of January, April, July and October, respectively. The dark shaded areas indicate the envelope of trend lines for the trends estimated based on all months of January, April, July and October, respectively. The light shaded areas show the associated envelope of 5/95th confidence intervals.

https://doi.org/10.5194/hess-2020-369
Preprint. Discussion started: 24 July 2020

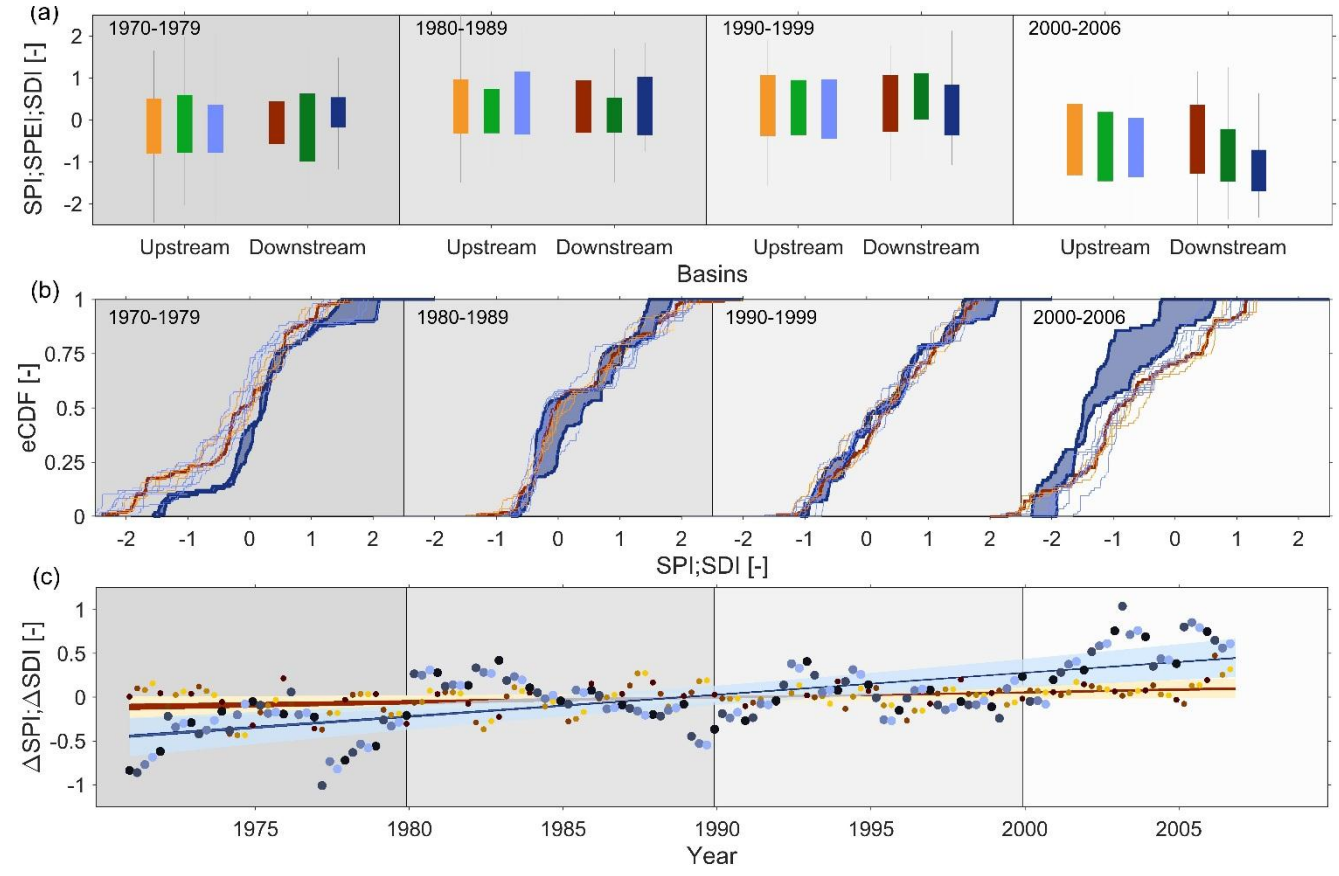

Figure 8. (a) decadal distributions of SPI, SPEI and SDI for the most upstream sub-basins (ID1-ID6) and the downstream sub-basins (ID7-ID8), (b) decadal empirical cumulative distribution functions of SPI (thins red lines upstream basins, bold red lines: downstream basins) and SDI (thin blue lines: upstream basins, bold blue lines: downstream basins). Note that the blue shaded area is added for better visualization of the shifts in downstream basins only and does not have a specific meaning. (c) time series of differences between mean upstream and mean downstream SPI (ΔSPI: yellow and red shades) as well as between mean upstream and mean downstream SDI (ΔSDI: blue shades). The symbols with shades from dark to light indicate the monthly SPI values (based on 12 months accumulation period) for the months January, April, July and October, respectively. The dark shaded areas indicate the envelope of trends in ΔSPI and ΔSDI, respectively, estimated based on all months of January, April, July and October, respectively. The light shaded areas show the associated envelope of 5/95th confidence intervals.

https://doi.org/10.5194/hess-2020-369
Preprint. Discussion started: 24 July 2020

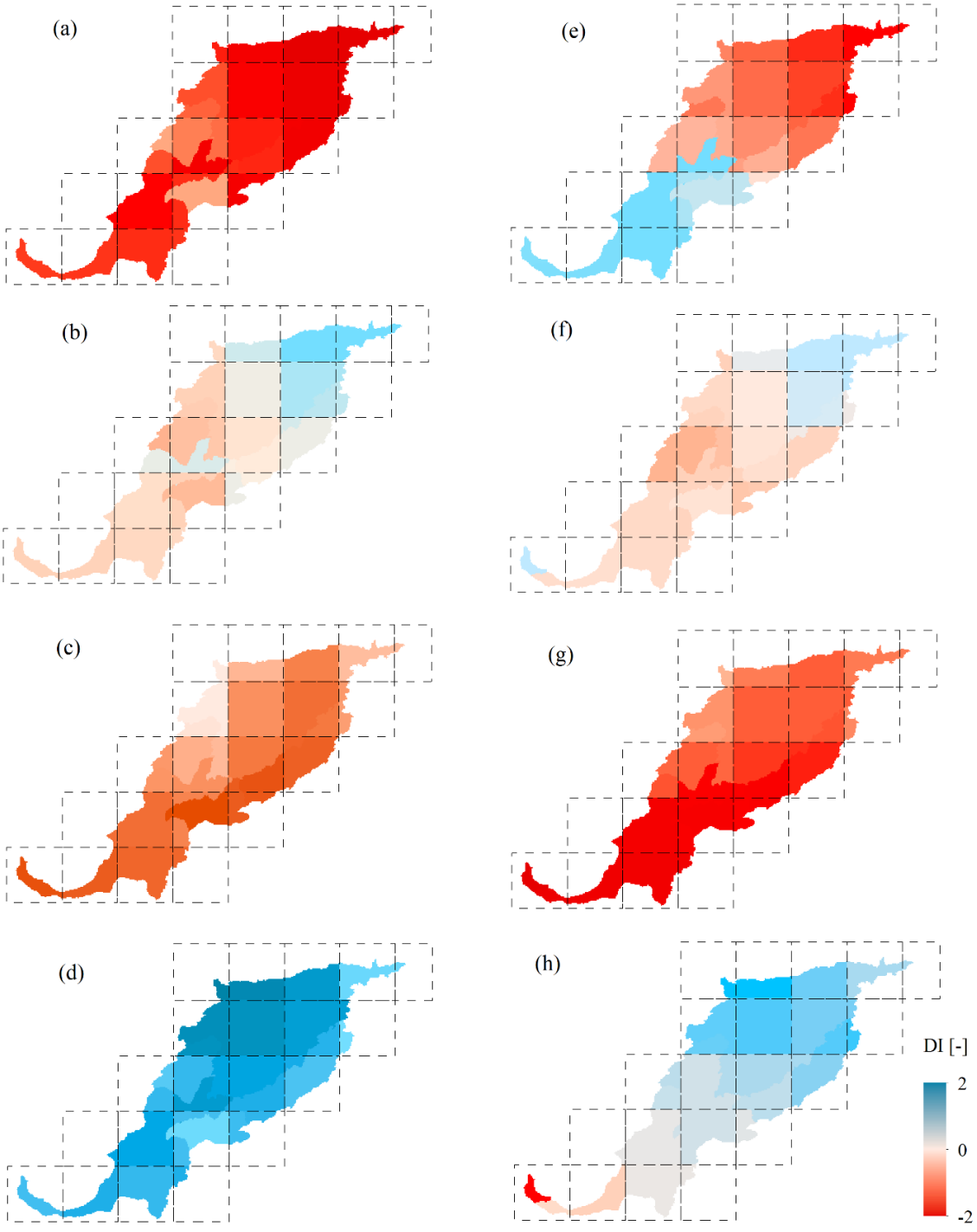

Figure 9. Spatial distribution of (a)-(d) SPI and (e)-(h) SDI for the years 1977, 1987, 2002 and 2003, based on the grid cells of the model application.

https://doi.org/10.5194/hess-2020-369
Preprint. Discussion started: 24 July 2020

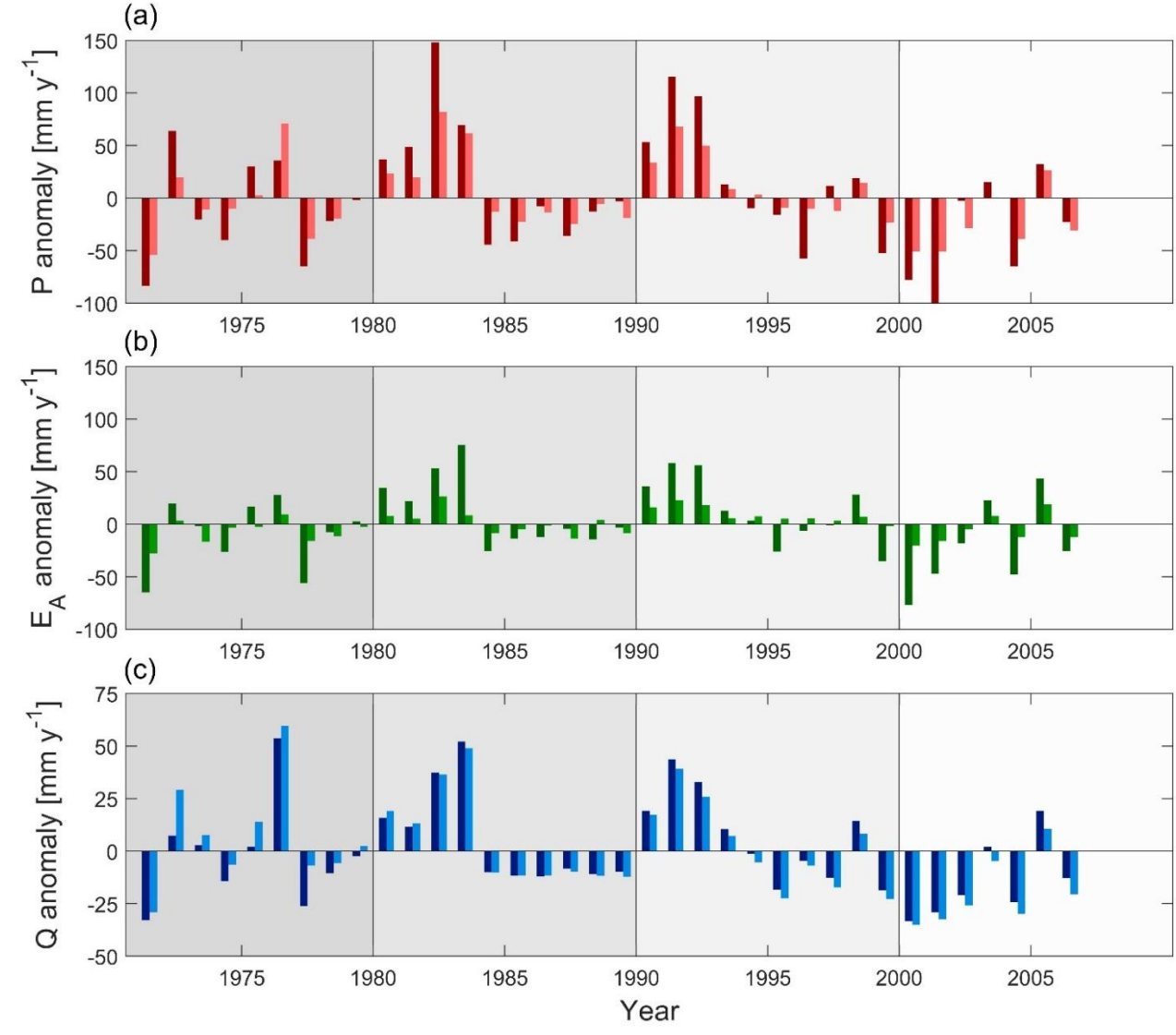

960 **Figure 10.** (a) Precipitation anomalies, (b) actual evaporation anomalies (here: $E_A = E_I + E_T$) and (c) streamflow anomalies over the study period. All anomalies are calculated based on the 1970-2006 mean values. The dark shaded bars indicate the combined flows to/from the upper basin (ID1-ID6), the light shaded bars show the flows to/from the lower basin (ID7).

965

https://doi.org/10.5194/hess-2020-369
Preprint. Discussion started: 24 July 2020

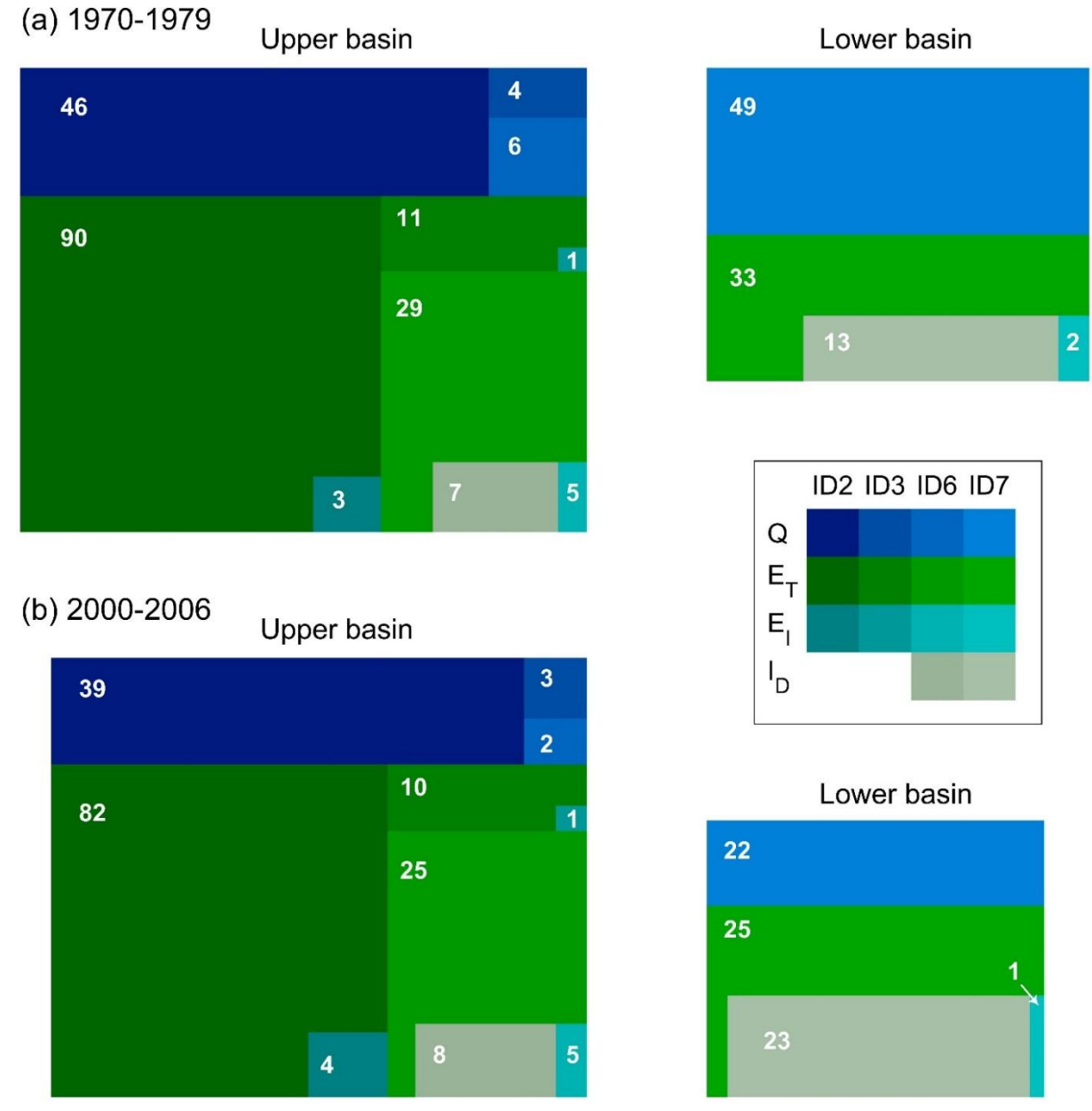

995 **Figure 11.** Water balances of the Upper and the Lower basins, respectively for (a) the 1970-79 and (b) the 2000-2006 periods. The size of the outer squares is equivalent to the total water available, i.e. for the upper basin precipitation P, for the lower basin precipitation P plus the combined inflow Q from the upper basin. The size of the internal rectangles of each flux (Q: streamflow, E_T: transpiration, E_I: interception evaporation and I_D: irrigation demand) in each sub-basin is equivalent to its fraction of the total available water in the upper and lower basin, respectively. The fluxes represent the decadal mean 1000 values and are shown in [mm y^{-1}].